Ore Geology Reviews 75 (2016) 284–303

Contents lists available at ScienceDirect

Ore Geology Reviews

journal homepage: www.elsevier.com/locate/oregeorev

Thermal profiles inferred from fluid inclusion and illite geothermometry from sandstones of the Athabasca basin: Implications for fluid flow and unconformity-related uranium mineralization

Haixia Chu *, Guoxiang Chi

Department of Geology, University of Regina, 3737 Wascana Parkway, Regina, SK S4S 0A2, Canada

ARTICLE INFO

Article history:
Received 8 August 2015
Received in revised form 10 December 2015
Accepted 14 December 2015
Available online 17 December 2015

Keywords:
Fluid flow
Thermal profile
Fluid inclusions
Illite
Athabasca basin
Unconformity-related uranium deposits

ABSTRACT

The Proterozoic Athabasca basin and underlying basement host numerous unconformity-related uranium deposits that were formed from extensive fluid circulation near the basement-cover interface. Although it is generally agreed that the mineralizing fluids were basinal brines, it is still unclear what driving forces were responsible for the circulation of the basinal fluids. Because different fluid flow driving forces are associated with different thermal profiles, knowing the basin-scale distribution of paleo-fluid temperatures can help constrain the fluid flow mechanism. This study uses fluid inclusions entrapped in quartz overgrowths and authigenic illite in sandstones from three drill cores (WC-79-1, BL-08-01, and DV10-001) in the central part of the Athabasca basin as thermal indicators of paleo-fluids in the basin. A total of 342 fluid inclusions in quartz overgrowths were studied for microthermometry. The homogenization temperatures (T_h) range from 50° to 235 °C, recording the minimum temperatures in various diagenetic stages. Temperatures estimated from illite geothermometry (121 points) range from 212° to 298 °C, which are systematically higher than (partly overlapping) the T_h values, suggesting that illite was precipitated in hotter fluids following the formation of quartz overgrowths. Neither the fluid inclusion T_h values nor the illite temperatures show systematic increase with depth in individual drill cores. This, together with the high illite temperatures that cannot be explained by burial at a normal geothermal gradient (35 °C/km), is interpreted to indicate that basin-scale fluid convection took place during the diagenetic history of the basin. Prolonged fluid convection is inferred to be responsible for delivering uranium (extracted from the basin or the upper part of the basement) to the unconformity, where uranium mineralization took place due to redox reactions associated with fluid-rock interaction or structurally controlled fluid mixing.

1. Introduction

Basin-scale fluid flow in sedimentary basins played a significant role in the formation of many mineral and petroleum deposits (Bethke and Marshak, 1990; Garven and Raffensperger, 1997; Cathles and Adams, 2005). The mechanism of such fluid flow, for example that responsible for the formation of Mississippi Valley-type (MVT) Zn–Pb deposits, has been a subject of scientific debates for over three decades, one of the focuses being whether or not a given fluid flow model can explain the heat anomaly observed in the deposits (Cathles and Smith, 1983; Anderson and Macqueen, 1988; Bethke and Marshak, 1990; Garven et al., 1993; Garven and Raffensperger, 1997; Cathles and Adams, 2005). This is understandable because fluid flow is always associated with heat transport, and different fluid flow mechanisms may result in different thermal profiles (Duddy et al., 1994; Deming, 1994; Jessop and Majorowicz, 1994; Phillips, 2009; Ingebritsen and Appold, 2012; Chi, 2015). Thus, the study of thermal profiles in sedimentary basins is important for constraining fluid flow models. Fluid flow mechanisms related to the formation of sedimentary basin-hosted (especially unconformity-related) uranium deposits have also been extensively studied (Sanford, 1992; Raffensperger and Garven, 1995a, b; Chi et al., 2011, 2013, 2014; Cui et al., 2010, 2012a, b; Chi and Xue, 2014), but so far little attention has been paid to the thermal effects of the fluid flow as was done for the MVT deposits.

The unconformity-related uranium (URU) deposits, which are best developed in Proterozoic basins in northern Canada and northern Australia, especially the Athabasca basin in northern Saskatchewan (Canada; Fig. 1a), represent the richest uranium deposits in the world (Jefferson et al., 2007; Fayek, 2013). The formation of these deposits has been related to circulation of large amounts of basinal fluids, facilitated by high permeabilities due to dominance of sandstones in the basins (Hoeve and Sibbald, 1978; Hoeve and Quirt, 1984; Wilson and Kyser, 1987; Kotzer and Kyser, 1990; Hiatt and Kyser, 2000; Cuney et al., 2003; Kyser et al., 2000; Richard et al., 2011, 2014; Mercadier et al., 2012). However, the driving forces controlling fluid flow are still controversial. Large-scale convection related to a normal geothermal gradient was proposed by Hoeve and Sibbald (1978) and Boiron et al.

* Corresponding author.
E-mail address: chu207@uregina.ca (H. Chu).

http://dx.doi.org/10.1016/j.oregeorev.2015.12.013
0169-1368/

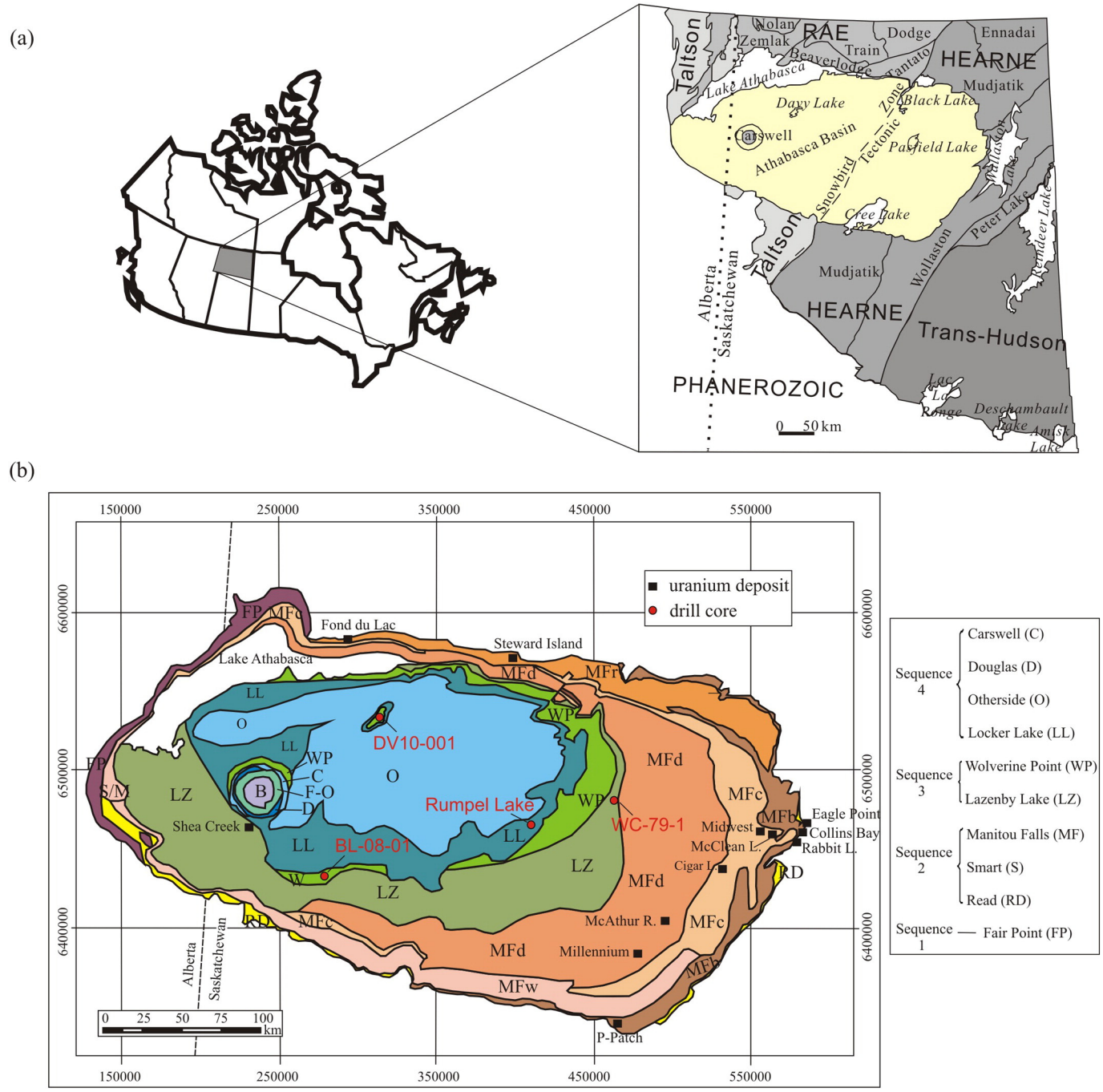

Fig. 1. (a) Location of the Athabasca basin in the regional tectonic framework (after Card, 2012). (b) Regional geological map of the Athabasca basin showing each formation, major uranium deposits, and the location of drill holes WC-79-1, BL-08-01, DV10-001, and Rumpel Lake (modified from Ramaekers et al., 2007, Jefferson et al., 2007; Bosman et al., 2011, 2012). B — basement; FP — Fair Point; S/M — undifferentiated Smart and/or Manitou Falls; RD — Read; MF — Manitou Falls (b — Bird; r — Raibl; w — Warnes; c — Collins; d — Dunlop); LZ — Lazenby Lake; W — Wolverine Point; LL — Locker Lake; O — Otherside; D — Douglas; C — Carswell; F–O — undivided Fair Point to Otherside formations. Note the UTM coordinate is used.

(2010) as the main mechanism responsible for fluid flow related to URU mineralization in the Athabasca basin, and was shown to be plausible using numerical modeling (Raffensperger and Garven, 1995a, b; Cui et al., 2010, 2012a, b). Topography-driven fluid flow was implied in some schematic models (Derome et al., 2005; Hiatt and Kyser, 2007; Boiron et al., 2010) and proposed to be responsible for URU mineralization in the Athabasca basin (Alexandre and Kyser, 2012). Both thermal convection and topography-driven flow are consistent with the near-hydrostatic fluid pressure regime in the Athabasca basin, as demonstrated by numerical modeling (Chi et al., 2013, 2014). Compaction-driven fluid flow was implied in hydrostratigraphic studies of sandstones of the Athabasca basin (Hiatt and Kyser, 2007), but it has been shown that such fluid flow was too slow to result in any significant thermal disturbance in the basin (Chi et al., 2013, 2014). Furthermore, based on the observation that most unconformity-related uranium deposits are spatially associated with faults crosscutting the unconformity, it was demonstrated that fluid flow related to uranium mineralization may be related to deformation along fault zones (Cui et al., 2012a), and mixed or alternative convection and deformation-driven fluid flow models have been advocated (Hoeve and Quirt, 1984, 1987; Raffensperger and Garven, 1995b; Cui et al., 2012a; Li et al., 2015). The uncertainties on fluid flow models related to URU mineralization are in part related to the poor understanding of thermal profiles related to fluid flow either at the basin scale or the deposit scale.

Various temperatures (ranging from 60° to 250 °C) have been estimated from fluid inclusions in quartz overgrowths, quartz veins and euhedral quartz for the basinal fluids and the mineralizing fluids in the Athabasca basin in previous studies (Pagel, 1975; Pagel et al., 1980; Kotzer and Kyser, 1995; Derome et al., 2005). However, most of these studies were focused on areas of mineralization, and the background temperatures of the basin, the ambient temperatures in the host rocks near the sites of mineralization and the temperatures of the actual mineralization fluids were not well distinguished. Ore-forming fluids were inferred to be hotter than the background diagenetic fluids in some studies (e.g., Kotzer and Kyser, 1995), and cooler in other studies (e.g., Derome et al., 2005). Few studies were carried out about the background thermal regime of the Athabasca basin. Pagel (1975) studied fluid inclusions entrapped in quartz overgrowths in sandstones from two long drill cores penetrating a major part of the stratigraphy of the Athabasca basin, and estimated that the burial temperature reached 180°C at the base of the Rumpel Lake drill core near the central part of the basin (Fig. 1b), and 220 °C at the base of and the MP-73-183 core near the Carswell structure in the central-west part of the basin. He further deduced a thermal gradient of 35 °C/km based on the assumption of a lithostatic pressure regime, a maximum burial depth of 4.8 km at the site of the Caswell structure, and a thickness of 3.2 km of eroded strata above the top of the Rumpel Lake drill core. Scott and Chi (2014) studied fluid inclusions in quartz overgrowths and illite in the sandstones from the Rumpel Lake drill core, and obtained higher maximum temperatures than those reported by Pagel (1975), mostly from 200° to 250 °C. Furthermore, they did not find the systematic increase of temperature with depth as inferred by Pagel (1975). Maximum burial temperatures of ~160° to 200 °C were obtained through a vitrinite reflectance study of the Douglas Formation near the top of the current Athabasca basin by Stasiuk et al. (2001), which are also hotter than those predicted by Pagel (1975)'s study (<130 °C).

In view of the controversies on basinal fluid flow models and discrepancies on burial temperatures and geothermal gradients in the Athabasca basin, a study of basin-wide distribution of paleo-temperatures both in horizontal and vertical directions is required. Such a study is best carried out in barren areas away from mineralization, so that the results represent the background thermal regime of the basin and can be used as a reference for comparison with the temperatures of the hydrothermal fluids in the mineralization areas. In this study, we collected 164 samples from three drill holes (WC-79-1, BL-08-01, and DV10-001) in the central part of the basin (Fig. 1b), which are widely spaced, far away from known mineralization and penetrate into the basement, and used fluid inclusion (in quartz overgrowths) microthermometry and illite (in interstitial space) geothermometry to characterize the paleo-temperatures during the diagenetic evolution of the sandstones. The results were used to construct vertical thermal profiles at different localities of the basin, to compare the thermal profiles from different localities, and to infer the fluid flow mechanisms that may explain the observed thermal profiles. Furthermore, the significance of the results for URU mineralization, in terms of fluid flow and metal extraction from source rocks, was explored.

2. Geological settings

The Athabasca basin in northern Saskatchewan and Alberta in Canada is located in the western Churchill Province between the eroded remnants of two major orogenic belts: the Taltson magmatic zone and Thelon tectonic zone in the west, and the Trans-Hudson Orogen in the east (Card, 2012; Fig. 1a). The crystalline basement rocks include the Taltson magmatic zone, the Rae Province, and the Hearne Province. The latter two are separated by the Snowbird tectonic zone (Hoffman, 1988; Card et al., 2007) beneath the center of the Athabasca basin. The Taltson magmatic zone, which separates the Rae Province from the Slave Province to the west (Hoffman, 1988), is composed of a variety of 1.99–1.92 Ga plutonic rocks and 3.2–2.14 Ga metamorphic complexes of amphibolites to granitic gneiss (Card et al., 2007). Both the Rae and Hearne provinces in Saskatchewan contain Archean granitoid gneiss (ca. 3.0 Ga) and supracrustal belts (>2.6 Ga), Paleoproterozoic metasedimentary rocks (1.8–2.45 Ga), and together with mafic to felsic intrusions, that were affected by the 2.0 to 1.9 Ga Thelon-Taltson and the 1.9 to 1.8 Ga Trans-Hudson orogenies (Card et al., 2007).

The non-metamorphosed sedimentary rocks in the Athabasca basin belong to the Athabasca Group, which are divided into four sequences separated by basin-wide unconformities (Hiatt and Kyser, 2007; Ramaekers et al., 2007; Fig. 1b). Sequence 1 (Fair Point Formation) and Sequence 2 (Read, Smart, and Manitou Falls formations) consist of conglomerate and quartz arenite, with minor mudstone. Sequence 3 (Lazenby Lake and Wolverine Point formations) is composed of sandstone, siltstone, and mudstone, and Sequence 4 (Locker Lake, Otherside, Douglas, and Carswell formations) comprises conglomeratic quartz arenite, quartz arenite, and pebbly quartz arenite in the Locker Lake and Otherside formations, mudstone and fine to very fine quartz arenite in the Douglas Formation, and carbonates with siliciclastic interbeds in the Carswell Formation (Ramaekers et al., 2007). The sedimentation in the Athabasca basin is inferred to have started after ca. 1750 Ma based on thermo-geochronological data of the Trans-Hudson Orogen (Annesley et al., 1997; Orrell et al., 1999; Alexandre et al., 2009; Kyser et al., 2000), which may represent the maximum age of the Fair Point Formation (Ramaekers et al., 2007). An age of 1740–1730 Ma has been proposed for the Manitou Falls Formation (Alexandre et al., 2009; Rainbird et al., 2006); a 1644 ± 13 Ma age was reported for igneous zircon in tuffaceous units in the Wolverine Point Formation (Rainbird et al., 2007), and a Re–Os isochron age of 1541 ± 13 Ma was obtained for carbonaceous shales in the Douglas Formation (Creaser and Stasiuk, 2007). The strata of the Athabasca basin are cut by the Mackenzie diabase dikes, which have been dated at ca. 1267 Ma (LeCheminant and Heaman, 1989).

Uranium deposits in the Athabasca basin occur near the sub-Athabasca unconformity, and are commonly associated with reactivated basement faults that cut and displace the unconformity (Hoeve and Sibbald, 1978; Hoeve and Quirt, 1984; Jefferson et al., 2007; Kyser and Cuney, 2008; Fayek, 2013). Uranium mineralization can be strictly basement-hosted (e.g. Rabbit Lake, P-Patch, Eagle Point, Millennium), unconformity-hosted (e.g. Midwest, Collins Bay, Cigar Lake), perched in the sandstones (e.g. Stewart Island, Fond du Lac), or a combination of two or more of these mineralization styles or locations (e.g., Shea Creek: basement + unconformity + perched; McArthur River: basement + unconformity; McClean Lake: unconformity + perched) (Jefferson et al., 2007; Fig. 1b). Primary uranium mineralization is inferred to have occurred at around 1590 Ma, based on LA–ICP–MS U–Pb dating of uraninite and Ar–Ar dating of syn-mineralization illite (Alexandre et al., 2009). The most important uranium deposits discovered so far are concentrated in the eastern margin of the basin, especially along the northeast-trending transition zone between the Mudjatik and Wollaston basement domains (Jefferson et al., 2007; Kyser and Cuney, 2008).

3. Drill cores examined and sampling

Three drill cores (WC-79-1, BL-08-01, and DV10-001) from the central part of the Athabasca basin (Fig. 1b) were selected for this study. The drill cores were logged in details to record lithological changes (Fig. 2), and a total of 164 core samples (40 from WC-79-1, 44 from BL-08-01, and 80 from DV10-001) from various depths were collected for petrographic and paleo-thermometric studies.

The WC-79-1 core, located near Pasfield Lake, was drilled by E&B Exploration in 1979 (Bosman et al., 2011). This 947 m deep drill penetrates the Lazenby Lake, Manitou Falls, and Read formations, and intersects the basement at a depth of 940 m. The thin basal Read Formation is mainly comprised of conglomeratic sandstone, and minor mudstone. The overlying Manitou Falls Formation consists of medium to coarse sandstone

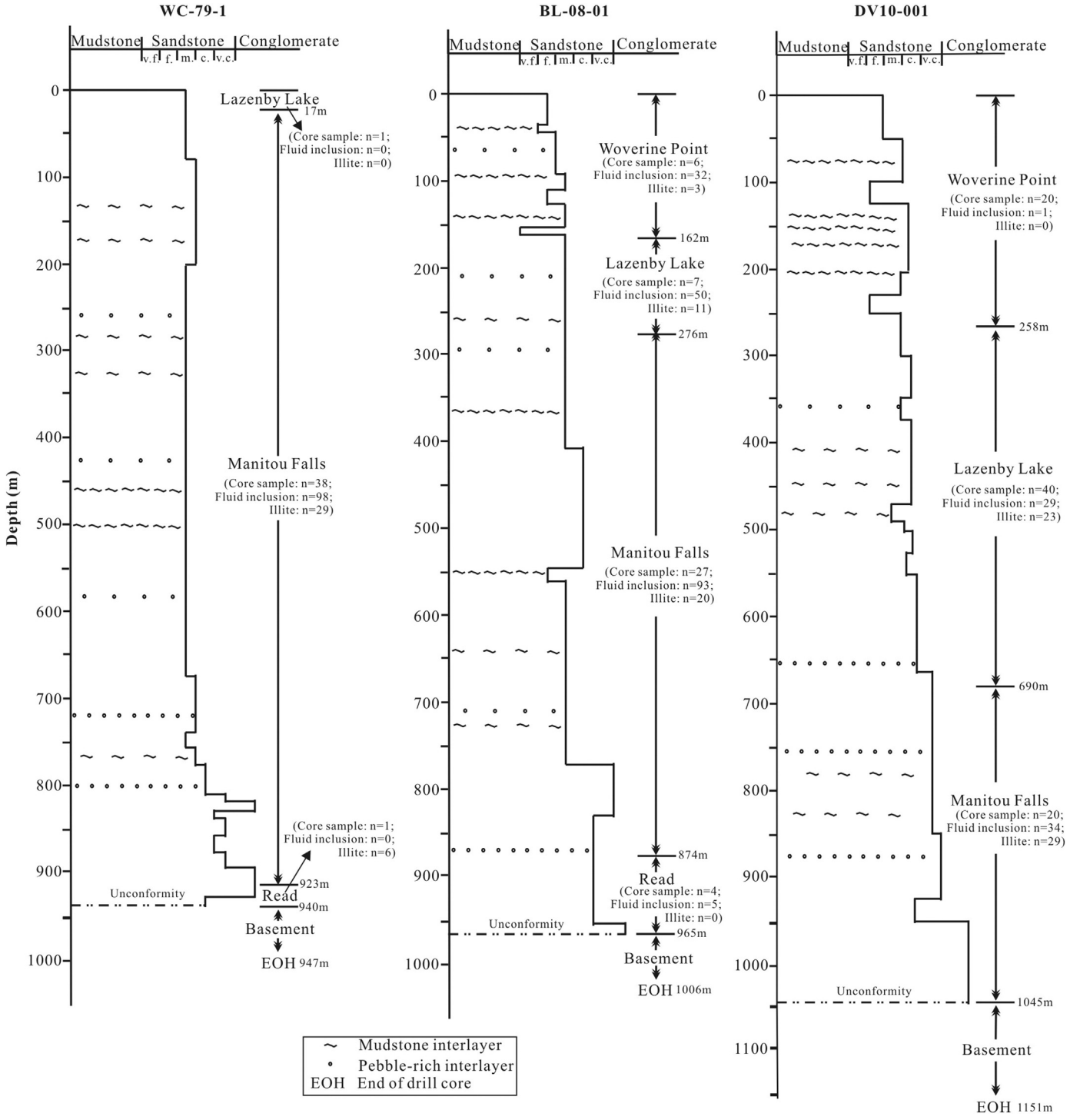

Fig. 2. Core logging of WC-79-1, BL-08-01, and DV10-001 drill holes (division of the formations is after Bosman et al., 2011, 2012), also showing the numbers of core samples, fluid inclusions examined and illite analyzed in each formation. v.f. = very fine grained; f. = fine grained; m. = medium grained; c. = coarse grained; v.c. = very coarse grained.

with variable amounts of conglomerate, mudstone intraclasts, and intercalated mudstone. The Lazenby Lake above is only about 10 m thick and consists of medium sandstone and minor intercalated mudstone.

The BL-08-01 core, located to the southeast of the Carswell Structure (Fig. 1b), was drilled by Bayswater Exploration in 2008 (Bosman et al., 2012). This core penetrated the Wolverine Point, Lazenby Lake, Manitou Falls, and Read formations from top to bottom with a total depth of 1006 m. The basement was intersected at a depth of 956 m. The Read Formation contains coarse to very coarse sandstone with variable amounts of conglomerate. The Manitou Falls Formation mainly consists of medium to coarse sandstone, with variable amounts of conglomerate, mudstone interclasts and intercalated mudstone. The Lazenby Lake Formation is composed of medium sandstone with minor mudstone and pebbly sandstones. The Wolverine Point Formation is made of fine to medium sandstone, with variable amounts mudstone intraclasts and intercalated mudstone, and minor pebbly sandstones.

DV10-001 is an exploration hole near Davy Lake drilled by Fission Energy Corp. in 2010 (Fission Energy Corp., 2012). It is approximately

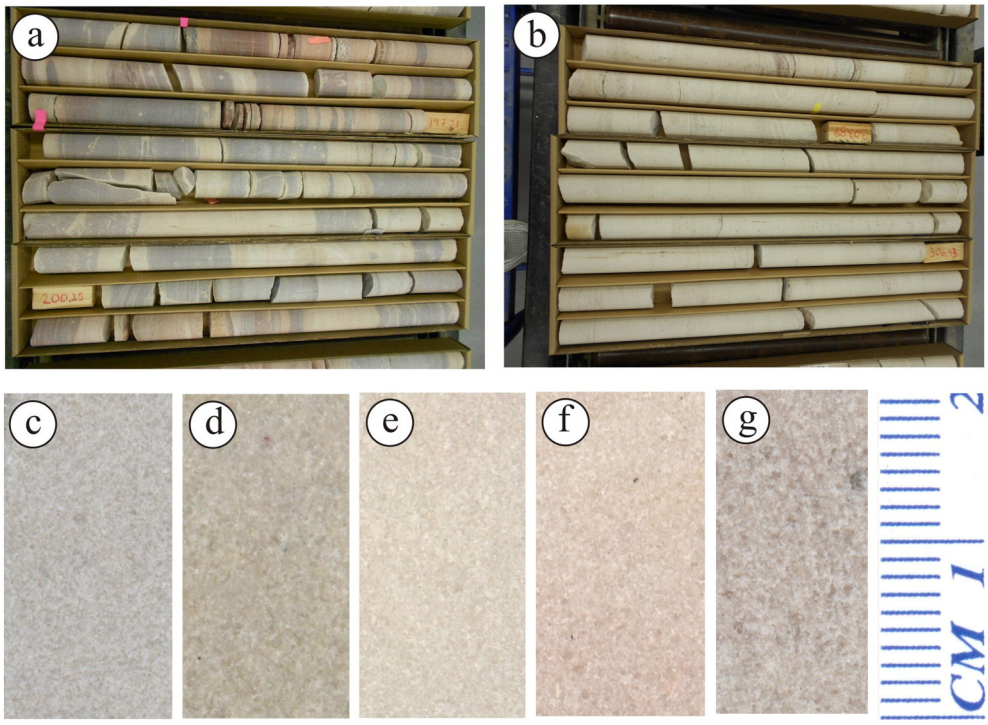

Fig. 3. Core samples from the WC-79-1, BL-08-01, and DV10-001 drill holes. a — light-colored intervals between dark gray or purple layers; b — massive light-colored layers; c — fine-grained, gray, sandstone from WC-79-1 drill core (sample 1409); d — medium-grained, yellow, sandstone from BL-08-01 drill core (sample 1452); e — coarse-grained, white, sandstone from BL-08-01 drill core (sample 1478); f — coarse-grained, pink, sandstone from DV10-001 drill core (sample 1250); g — coarse-grained, gray, sandstone from BL-08-01 drill core (sample 1455). (For interpretation of the references to color in this figure legend, the reader is referred to the web version of this article.)

40 km away from any previous drill hole in the basin and is the closest hole to the center of the basin (Bosman et al., 2012; Fig. 1b). The drill core is 1151 m deep in total, penetrates the Wolverine Point, Lazenby Lake, and Manitou Falls formations, and intersects the sub-Athabasca unconformity at a depth of 1045 m (Bosman et al., 2012). Based on core logging, the Manitou Falls Formation consists mainly of coarse to very coarse sandstone, with significant amounts of conglomerate near the base, and minor amounts of mudstone intraclasts and intercalated mudstone in the middle and upper part. The Lazenby Lake Formation comprises medium to coarse sandstone with intercalated conglomerate and mudstone, whereas the Wolverine Point Formation consists of fine to medium sandstones with variable amounts of mudstone.

Overall, the strata penetrated by these three drill holes mainly consist of sandstones with variable amounts of mudstones and conglomerates. More mudstones were observed in the Wolverine Point Formation, while more pebbly layers and conglomerates were found in the Manitou Falls and Read formations (Fig. 2). Sandstones are fine to coarse grained and characterized by widespread redbed layers (purple, brown, red or dark red; Fig. 3a). A significant proportion of these redbed layers were bleached to relatively light colors (pink, yellow, buff or gray; Fig. 3b–g) because of bleaching or removal of iron oxides and/or hydroxides (IOH; Chu et al., 2015). Bleaching likely took place at a late diagenetic stage after significant compaction, as reflected by the sharp boundaries between the redbeds and bleached parts (Fig. 3a). The bleached parts tend to be slightly better cemented than the non-bleached parts (Chu et al., 2015). Sandstone samples from different formations and depths (Fig. 2), including redbed and bleached parts, were collected and examined in this study.

4. Analytical methods

This study uses fluid inclusion microthermometry and illite geothermometry to evaluate the paleo-temperatures of basinal fluids in the diagenetic records. Homogenization temperatures of fluid inclusions represent the minimum entrapment temperature (Roedder, 1984), and illite crystal structure and composition can be used to estimate the formation temperature (Essene and Peacor, 1995). Polished thin sections were used for petrographic observation and illite analysis, and doubly-polished sections were used for fluid inclusion studies.

All thin sections were examined by conventional transmitted light and reflected light microscopes for petrographic studies. Scanning electron microscope–energy dispersive spectroscopy (SEM-EDS) was used as an auxiliary tool to check some unknown minerals. The HF staining method was applied to discern quartz and potential feldspars (Bailey and Stevens, 1960).

Fluid inclusion microthermometry was conducted at the Geofluids Laboratory, University of Regina, using a Linkam THMGS600 heating-freezing stage, which was calibrated using synthetic fluid inclusions of known compositions. Homogenization temperatures (T_h), halite-melting temperatures ($T_{m\text{-halite}}$), and ice-melting temperatures ($T_{m\text{-ice}}$) were measured with a precision (reproducibility) of ± 1 °C, ± 1 °C, and ± 0.1 °C, respectively. Homogenization temperatures were measured before cooling runs to avoid the effect of potential artificial stretching due to ice crystallization. Ice-melting temperatures were used to calculate the salinities of liquid-vapor fluid inclusions using the equations of Chi and Ni (2007), whereas halite-melting temperatures together with ice-melting temperatures were used to estimate salinities of halite-bearing fluid inclusions according to the program by Steele-MacInnis et al. (2011).

Individual illite crystals filling interstitial space in sandstones were analyzed for major element composition with electron microprobe analysis (EMPA) technique at the University of Manitoba. A CAMECA SX100 electron microprobe was used with a Princeton Gamma Tech Energy Dispersive Spectrometer (PGT EDS) and five wavelength dispersive X-ray spectrometers (WDS). Operation conditions were set at a voltage of 15 kV and a beam current of a 20 nA. Element calibration standards were diopside for Si and Ca, andalusite for Al, albite for Na, orthoclase for K, olivine for Mg, and fayalite for Fe. The values of the element oxides

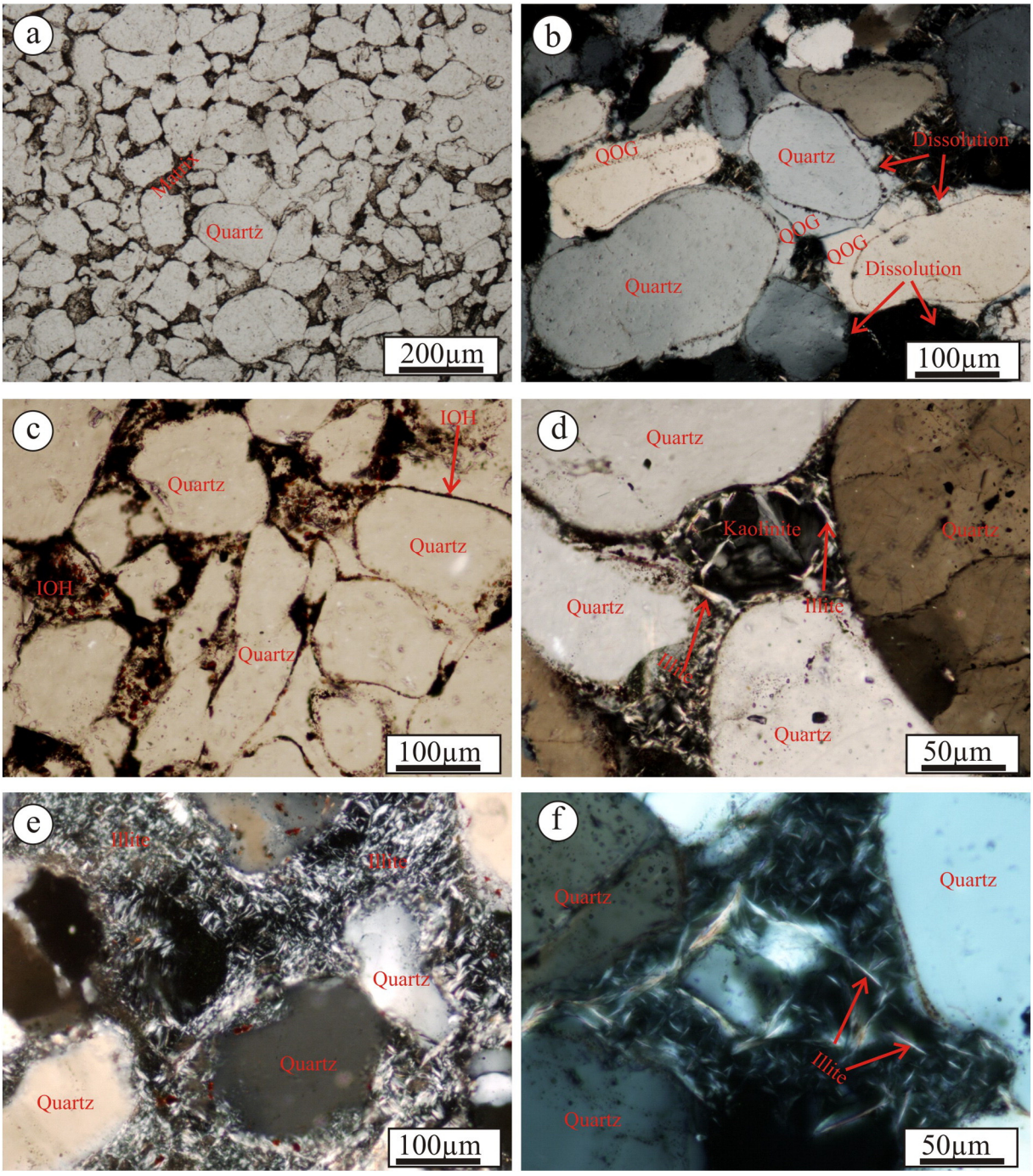

Fig. 4. Photomicrographs of sandstones showing occurrence of quartz and illite. a — typical sandstone composed of quartz with minor matrix, sample 1469 from BL-08-01 drill core; b — detrital quartz and quartz overgrowth (QOG), also showing dissolution of quartz overgrowth, sample 1217 from DV10-001 drill core; c — early iron oxide–hydroxides (IOH) in the dustline coating the detrital quartz and late IOH dispersed between quartz grains, sample 1226 from DV10-001 drill core; d — illite replacing kaolinite, sample 1227 from DV10-001 drill core; e — aggregates of illite (cement and replacement) filling interstitial space between detrital quartz grains, sample 1354 from DV10-001 drill core; f — illite crystals (cement) filling pores between quartz grains, sample 1414 from WC-79-1 drill core.

were converted into structural formulas of illite (K, Na, Ca) $(Al, Mg, Fe)_2(Si, Al)_4O_{10}(OH)_2$. K, Na, and Ca were all allocated to the interlayer site, whereas Si and Al were assigned to the tetrahedral layer. The remainder of the Al, together with all Mg and Fe were assigned to the octahedral layer. The proportions of six end-member minerals, muscovite, paragonite, Ca-paragonite, Fe-celadonite, Mg-celadonite, and pyrophyllite were calculated following the method of Cathelineau (1988), and the crystallization temperatures of illite were estimated using the equation $X_{Pyroph} = -0.0025\,T\,(°C) + 0.7928$ derived by Cathelineau (1988). Illite formation temperatures were also calculated using an alternative equation $T\,(°C) = 267.95x + 31.50$, (where $x = K + |Fe–Mg|$) from Battaglia (2004) for comparison.

5. Petrography and paragenesis

Petrographic studies indicate that the sandstones from the three examined drill cores are mainly composed of detrital quartz grains (Fig. 4a–b), with minor amounts of muddy matrix, iron oxide-hydroxide (IOH) (Fig. 4c), and clay minerals (Figs. 4d–f). Zircon and tourmaline grains were observed locally. No K-feldspar or plagioclase grains

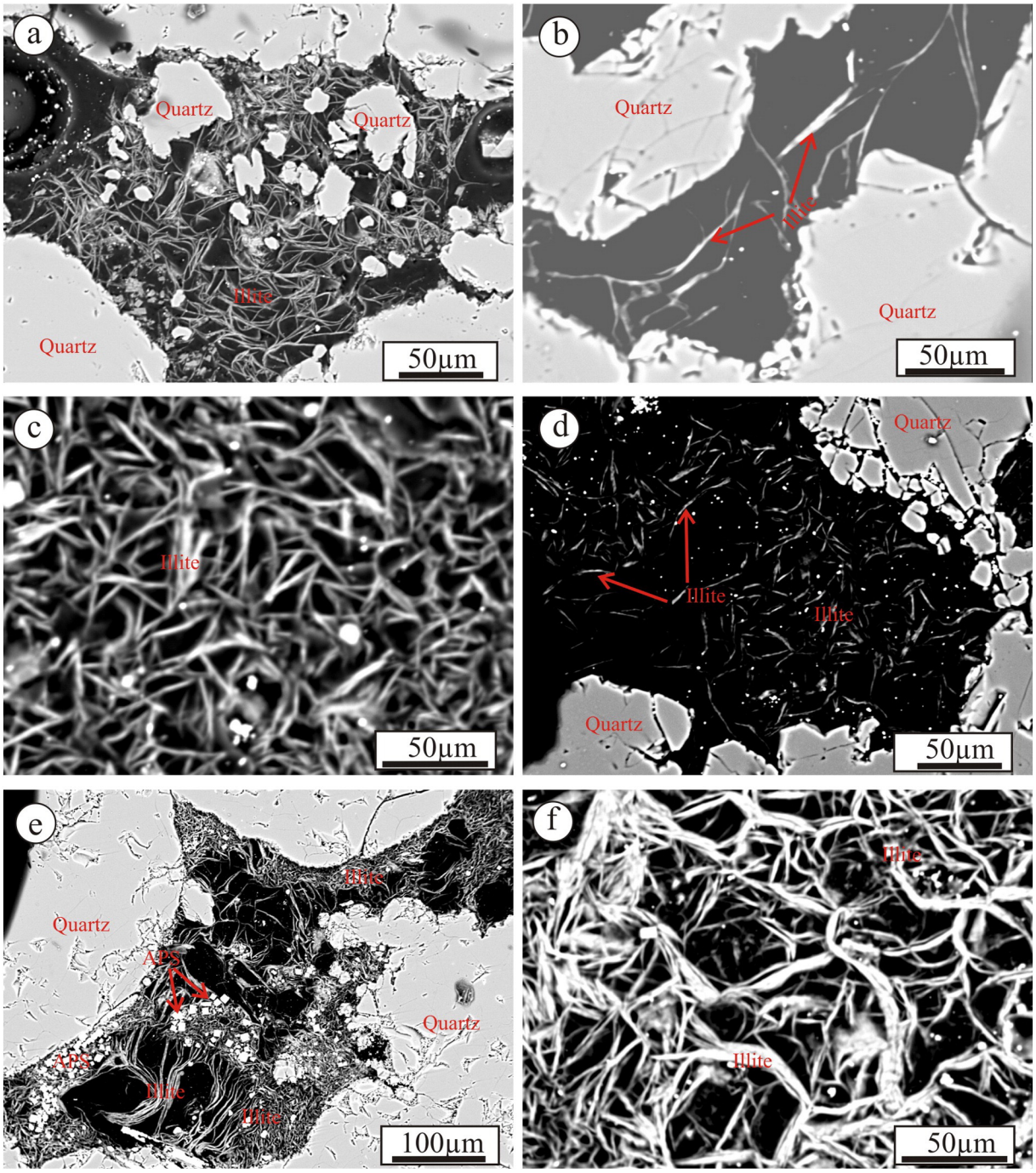

Fig. 5. BSE images illustrating the occurrences of authigenic illlite. a — very thin illite crystals filling the pore space between quartz grains, sample 1411 from WC-79-1 drill core; b — isolated thin illite crystals distributed in the pore space, sample 1414 from WC-79-1 drill core; c — densely intergrown thin illite crystals in pore space, sample 1457 from BL-08-01 drill core; d —very thin illite crystals randomly dispersed in the pore space, sample 1479 from BL-08-01 drill core; e — curved illite crystals associated with disseminated APS particles, sample 1360 from DV10-001 drill core; f — thin and thick illite crystals tangling together, sample 1360 from DV10-001 drill core.

were found in any of the samples examined. The sandstones are mostly well compacted and cemented, with long and convex-concave grain-to-grain contacts.

Authigenic quartz overgrowths, separated from the detrital grains by the dustlines (Figs. 4b–c), are well developed in most stratigraphic intervals. Early diagenetic micro-quartz cements reported by other researchers (Hiatt et al., 2007) are rare in the samples examined. The thicknesses of quartz overgrowths range from a few micrometers to more than one hundred micrometers (Fig. 4b–c). Both detrital quartz grains and quartz overgrowths commonly show dissolution features, such as embayments (Fig. 4e) and incomplete edges (Fig. 4b–c), but no discontinuity related to dissolution can be discerned within individual quartz overgrowths.

Clay minerals (kaolinite/dickite and illite) commonly filled interstitial spaces (Figs. 4d-f and 5). Illite occurs as replacement of previous kaolinite (Fig. 4d) and detrital muscovite, and as cements filling interstitial space (Figs. 4e–f and 5). All the illite crystals are needle-like, either as isolated crystals (Figs. 4f, 5b and d) or aggregates (Figs. 4e, 5a, c, and f). Most illite crystals are less than 1 μm thick, and some of them can reach about 1-2 μm (Fig. 5f). Minor amounts of aluminum phosphate–sulfate (APS) were locally found disseminated among illite crystals (Fig. 5e).

Table 1
Microthermometric results of fluid inclusions in quartz overgrowth from sandstones of the Athabasca basin.

Sample #	Depth (m)	FI #	Occurrence	Size (μm)	V (%)	T_{m-ice} (°C)	Salinity (wt.%)	T_h (°C)
WC–79–1 drill core								
1404	63.4	b	Isolated	6	10			192
		c	Short trail	6	12	–21.1	23.1	103
		e	Short trail	8	10	–21.3	23.2	123
		f		10	10	–21.5	23.3	112
1406	112.5	a	Isolated	10	10	–27.5	25.1	167
		d	Isolated	6	10	–35.2	27.3	162
1407	138.0	b	Isolated	8	10	–25.0	24.3	155
		c	Isolated	10	10	–23.3	23.8	183
1408	170.6	b	Dustline	7	10	–25.2	24.4	125
1410	246.5	a	Dustline	6	12	–29.5	25.7	141
1416	364.3	a	Dustline	14	10	–11.1	15.1	129
		ai	Dustline	12	10			50
		b	Dustline	6	10			161
		c	Dustline	5	10			188
		d	Dustline	20	12	–25.9	24.1	124
1419	440.1	a	Dustline	12	8			66
		c	Dustline	10	8	–29.0	25.5	107
		d	Dustline	10	10	–24.8	24.3	110
1420	457.0	b	Dustline	8	10			70
1421	475.5	a	Dustline	8	8			66
		b	Dustline	8	10	–17.4	20.5	121
		c	Dustline	12	10			69
		d	Dustline	10	10	–25.6	24.5	120
		e	Dustline	10	12	–20.0	22.4	164
		f	Dustline	10	10	–19.2	21.8	62
1422	502.8	a	Isolated	6	10			133
		b	Isolated	10	10			123
		c	Isolated	6	10			106
		d	Isolated	10	10	–21.1	23.1	103
		e	Dustline	7	10			112
1423	526.3	a	Dustline	24	10	–20.0	22.4	78
		b	Cluster	20	10			70
		c		18	10	–17.0	20.2	61
		d	Dustline	8	10			84
		e		6	10			73
		f	Isolated	10	10			114
1425	576.5	a	Dustline	8	10	–29.2	25.6	96
		b	Dustline	8	10	–17.0	20.2	198
		c	Dustline	14	12	–25.3	24.4	132
1426	593.1	a	Isolated	14	10	–29.8	25.7	76
		b	Dustline	10	10	–35.5	27.4	64
		c	Dustline	10	8	–34.1	27.0	115
		d	Isolated	10	12	–23.6	23.9	170
		e	Dustline	12	12			123
		f	Dustline	10	8			71
		g	Dustline	6	10			129
		h	Dustline	6	10			152
1427	601.2	a	Dustline	10	8	–22.8	23.7	75
		b	Dustline	10	8			77
		c	Dustline	14	10	–24.8	24.3	114
		d	Dustline	10	10			95
		e	Dustline	16	10			69
		f	Dustline	12	10	–29.9	25.8	58
1428	613.7	a	Dustline	14	10			66
		b	Dustline	10	10			70
		c	Isolated	20	12			97
1429	647.2	a	Dustline	8	10	–30.4	25.9	115
		b	Dustline	10	10	–22.5	32.6[a]	50
1431	693.8	b	Dustline	6	10			94
		c	Dustline	10	10			67
		d	Dustline	10	10			63
		f	Dustline	12	10	–24.7	24.2	96
1432	747.4	a	Dustline	14	10			64
		b		18	10	–23.3	23.8	65
		c	Isolated	12	10	–31.5	26.2	84
		d	Dustline	10	10	–32.5	26.5	55
		e	Dustline	14	10	–30.1	25.8	73
		f	Dustline	7	10			119
		g	Dustline	5	12			132
1432	747.4	h	Dustline	6	15			182
1433	768.9	a	Dustline	8	12	–25.2	24.4	141
		b	Dustline	8	10	–37.9	28.1	140
		c	Isolated	10	12	–31.5	26.2	149
1434	792.0	b	Dustline	8	10			92
		c	Dustline	12	10			63
1435	805.0	a	Dustline	5	12			218
		b	Dustline	8	12	–34.2	27.0	162
		c	Dustline	10	12			124
		d	Dustline	6	12	–37.2	27.9	88
1436	845.8	a	Isolated	7	10			205
		c	Dustline	6	10			149
		d	Isolated	8	10	–24.1	24.1	92
		e	Dustline	12	10			106
		f		10	10			112
1437	866.0	a	Dustline	10	12	–24.9	24.3	135
		b	Dustline	6	10			93
		c	Dustline	12	10	–33.1	26.7	57
		d		8	10	–24.8	24.3	52
		e	Dustline	6	12			156
		f	Dustline	10	10	–44.3	29.8	110
		g	Dustline	6	12			84
		h		8	10			76
		i	Isolated	16	10			87
1438	892.5	a	Dustline	6	10			89
		b	Dustline	8	10			50
		c	Dustline	10	10	–25.0	24.3	85
		d	Isolated	12	10	–9.2	13.1	82
		f	Dustline	14	10	–25.0	24.3	72
BL–08–01 drill core								
1441	41.5	a	Isolated	6	10			124
		b	Dustline	4	10			112
		c	Dustline	5	10			130
		d	Dustline	7	10			139
		e	Dustline	8	10			120
		f	Dustline	10	12	–28.0	25.2	153
		g		6	10			150
		i	Isolated	5	10			98
1442	57.2	a	Dustline	10	10	–9.9	13.8	57
		b	Dustline	14	10	–25.7	31.0[a]	88
		c	Dustline	6	10			93
		d	Dustline	7	10			130
		e	Dustline	12	10	–28.2	32.9[a]	89
1443	72.3	a	Isolated	8	10	–35.3	27.3	143
		b	Dustline	8	10			75
		d	Dustline	8	10			50
		e		8	10			63
1444	88.0	a	Dustline	10	10			67
		b		6	10			154
		bi	Dustline	8	10			138
		c		14	12	–26.3	24.7	144
		d	Dustline	7	10			86
1446	132.0	a	Dustline	8	10	–19.6	22.1	65
		b		6	10			71
		c		8	10			95
		d	Dustline	6	10			94
		e		8	10			98
		g	Dustline	8	10			73
		h	Dustline	7	10	–20.3	22.6	63
		i	Dustline	10	10	–31.9	26.4	67
		j	Dustline	12	10	–24.6	31.9[a]	50
1447	169.2	a	Dustline	12	12	–23.0	23.7	112
		b	Dustline	10	10	–25.6	24.5	114
		c	Cluster	8	10			109
		d		6	10			106
		e	Dustline	8	10			85
		ei		12	10	–24.6	24.2	93
		f	Dustline	10	10			78
		g	Dustline	6	10			150
		j	Dustline	10	10	– 30.3	32.1[a]	132
1448	174.3	a	Dustline	6	10			89
		b	Cluster	16	12	–37.2	27.9	127
		c		14	12	–35.0	27.3	129
		d	Dustline	6	10			146
		e	Dustline	5	10			92
		f	Isolated	18	10			81
		g	Dustline	8	10	–23.3	23.8	156
1449	199.3	a	Dustline	8	12			98
		c	Dustline	10	10			89
		d		8	10			83
		e	Dustline	6	10			72
		f	Isolated	8	10	–24.0	24.0	68
		g	Dustline	7	10			83
1450	214.5	a	Cluster	6	10			76
		b		5	10			74
		c	Dustline	6	10			146
		d	Isolated	14	10			65
		e	Isolated	10	10	–32.8	26.6	93
		g	Dustline	8	10			95
		h		8	10	–30.1	25.8	89
		i	Dustline	12	10			75
1451	225.4	a	Dustline	10	10			88
		b	Dustline	8	10	–26.1	24.6	106
		c	Dustline	10	10			83
		d	Dustline	8	10			78
		e	Isolated	6	10			113
		f	Dustline	6	10			123
		g	Dustline	8	10			89
1452	250.8	a	Isolated	6	10			107
		b	Isolated	6	10			117
		c	Dustline	8	10			69
		e	Cluster	8	10			87
		f	Isolated	8	10			182
		g	Dustline	6	10			119
1453	267.7	a	Isolated	12	10			107
		b	Dustline	12	10			114
		c	Isolated	5	10			121
		d	Dustline	7	10			138
		e	Dustline	8	10			58
		f	Dustline	8	10			135
		g		6	10	–42.5	29.3	148
		i	Dustline	8	10	–22.2	23.5	163
1454	283.5	j		6	10			129
		k	Cluster	8	10			120
		m		10	10			120
		n		5	10			125
		o	Dustline	10	10			103
		p	Dustline	10	10			128
1455	291.0	a	Dustline	14	10	–24.8	24.3	132
		b	Dustline	7	10			126
		d	Dustline	8	10			107
		e	Dustline	14	10	–24.6	24.2	64
		f	Dustline	12	10			77
		g	Dustline	10	10			102
1456	309.0	c	Cluster	10	10			102
		d	Dustline	6	12			98
		e	Dustline	12	12			98
		f	Dustline	10	10	–24.3	24.1	172
1457	321.6	a	Isolated	8	10			115
		b	Dustline	8	10			112
		c	Dustline	10	10			79
		d	Dustline	8	10	–25.5	24.5	154
1458	335.0	a	Isolated	10	10			123
		b	Isolated	6	10			127
		d	Cluster	6	10			142
1459	347.1	b	Cluster	7	15			123
		c	Cluster	6	12			140
		ci	Cluster	6	10			120
		di	Isolated	6	10			90
		e	Dustline	10	12			176

T_{m-ice} — ice melting temperatures; Salinity — calculated from equation of Chi and Ni (2007) using corresponding ice melting temperatures; T_h— homogenization temperatures.[a] Halite-bearing fluid inclusion; salinity was calculated according to their halite-melting temperatures (1429b–218 °C; 1442b–156 °C; 1442e–179 °C; 1446j– 189 °C; 1447j–141 °C; 1215d–198 °C) and the corresponding ice-melting temperatures using the program by Steele-MacInnis et al. (2011).

IOH occurs as dotted assemblages within the dustlines between detrital quartz and quartz overgrowths, or as platy or needle-like crystals between detrital quartz grains (Fig. 4c). Reddish sandstones are relatively enriched in matrix and IOH, whereas the bleached counterparts contain slightly more quartz overgrowths and illite.

Table 1 (*continued*)

Sample #	Depth (m)	FI #	Occurrence	Size (μm)	V (%)	T_{m-ice} (°C)	Salinity (wt. %)	T_h (°C)
1459	347.1	h	Dustline	12	10			108
		i		12	10			102
		j	Isolated	10	10			128
1460	365.1	a	Dustline	8	10			90
		b	Dustline	8	12			199
		c	Dustline	6	10			142
		d	Isolated	6	10			105
		e	Dustline	7	10			128
		g	Cluster	6	10			184
		h		6	10			175
1463	454.9	a	Dustline	7	10			199
1464	477.0	a	Dustline	6	10			105
1465	511.1	a	Isolated	6	10			158
1466	539.7	a	Dustline	6	10			210
1467	585.3	a	Dustline	6	10			86
		b	Dustline	6	12			185
1469	655.4	a	Dustline	8	10			169
		c	Dustline	8	10			143
1470	670.1	a	Dustline	8	12	–34.5	27.1	152
		b	Dustline	6	10			146
		c	Isolated	6	10			147
		d	Dustline	6	10			90
1471	678.7	a	Dustline	6	10			98
		b	Dustline	6	12			127
		c	Dustline	6	10			132
		d	Dustline	6	12			144
1472	691.6	a	Isolated	14	10			94
		b	Dustline	7	10			131
		c	Dustline	10	10			87
		d	Dustline	10	10			90
1473	717.2	a	Dustline	12	10	–25	24.3	82
		b	Dustline	8	10			101
		c	Dustline	8	10			74
		d	Isolated	6	10			115
		e	Dustline	12	10			96
		f	Dustline	8	10			137
		g	Dustline	8	10			104
		i	Dustline	10	12	–21.9	23.4	188
		j	Dustline	10	15	–17.0	20.2	172
		l	Dustline	8	10	–25.9	24.6	110
1474	748.5	a	Dustline	8	10	–40.6	28.8	117
		b	Dustline	10	10			120
		d	Dustline	8	10			109
1476	788.9	a	Isolated	10	10			101
		b	Dustline	6	10			145
1476	788.9	c	Isolated	8	10			89
		d	Dustline	8	10			70
1477	828.4	a	Dustline	6	12			154
		b	Dustline	5	10			72
		c	Dustline	6	10			159
		d	Dustline	8	10			85
		e	Dustline	6	10			98
		g	Dustline	10	10			96
		i	Dustline	8	10	–18.2	21.1	154
		j	Dustline	10	10			90
1478	847.9	a	Dustline	8	12			147
		b	Dustline	8	10	–28.5	25.4	84
		c		8	10	–38.6	28.3	124
		d	Dustline	8	10	–28.2	25.3	125
		e		6	12			131
		f	Dustline	8	10			235
		g	Dustline	8	10			132
1479	866.6	a	Dustline	6	10			79
		c	Dustline	8	12	–25.7	24.5	205
		d	Dustline	10	12	–48.6	30.7	78
1480	883.0	a	Dustline	8	10	–29.2	25.6	110
1484	963.0	a		6	10			136
		c	Dustline	8	10			139
		d		10	12			132
		e	Dustline	8	10			118
DV10– 001 drill core								
1215	297.7	a	Isolated	8	10			75
		b	Dustline	8	10			65
		c	Dustline	8	10	–20.7	22.9	111
		d	Isolated	10	10	–23.7	32.0[a]	70
		e	Dustline	10	10			90
1216	313.8	a	Isolated	6	10	–21.5	23.3	154
		c	Cluster	6	10	–31.0	26.1	173
		d		6	10	–26.0	24.6	182
		e	Cluster	10	10			79
		f		6	10			75
1235	682.4	a	Isolated	6	10			75
		b	Isolated	8	10	–26.0	24.6	94
1237	714.1	c	Dustline	6	10	–23.9	24.0	92
		d	Dustline	10	12	–25.3	24.4	150
		e	Dustline	6	10	–24.0	24.0	175
1238	726.7	a	Dustline	8	12	–38.0	28.1	156
		b	Dustline	6	12			80
1239	741.8	a	Isolated	8	10	–37.2	27.9	119
1241	778.3	a	Isolated	6	10			91
		b	Isolated	6	10			122
		c	Isolated	10	10	–24.5	24.2	90
1241	778.3	d	Dustline	10	10	–22.5	23.6	79
		e	Dustline	6	12			137
		f	Dustline	10	10	–26.8	24.9	155
		g	Isolated	7	10	–24.9	24.3	72
1246	878.7	a	Dustline	12	10	–38.1	28.1	117
		b	Dustline	7	12			170
		bi	Isolated	5	10			142
		c	Dustline	10	10	–33.9	26.9	192
		d	Dustline	8	10	–25.5	24.5	198
1249	915.0	c	Isolated	8	10	–7.5	11.1	87
		e	Dustline	10	10	–28.0	25.2	98
1250	935.0	a	Cluster	10	10	–25.2	24.4	85
		b		8	10	–27.0	24.9	76
1254	1021.3	b	Dustline	6	10	–33.2	26.7	102
		d	Dustline	7	10	–25.2	24.4	109
		e	Dustline	6	12			202
		f	Dustline	14	10	–33.8	26.9	173
		g	Dustline	8	10			97
		h	Isolated	6	10			126
1314	251.2	b	Isolated	6	10			108
1336	491.3	a	Dustline	6	10			75
		b	Dustline	7	10			83
1337	508.0	a	Dustline	7	10	–38.2	28.1	100
		b	Dustline	7	10			80
		c	Isolated	12	10			147
		d	Isolated	7	10			167
1340	561.2	a	Dustline	14	10	–31.8	26.3	79
		b	Dustline	16	10			100
		c		6	10			92
		e	Isolated	12	15	–34.5	27.1	203
1341	600.3	a	Isolated	6	10			103
		b	Dustline	6	10			125
		c	Dustline	7	10			102
		d	Isolated	6	10			115
1346	666.7	a	Dustline	6	10			147
		c	Dustline	6	10	–31.2	26.1	187
		e	Isolated	6	10			195
1349	765.3	a	Dustline	8	12	–22.5	23.6	178
		ai	Dustline	10	10			142
		b	Dustline	6	10			105
		bi	Dustline	6	10			114
		c	Dustline	6	12			184
1353	843.9	a	Dustline	6	10			98

A general paragenetic sequence, based on petrographic observations, is summarized as follows. The terms of "early diagenesis" and "late diagenesis" were used to describe the relative timing of diagenetic events, with the former referring to the stage when the sediments had not been subjected to significant compaction, and the latter to the stage when the sediments were solidified. Detrital components including quartz grains, matrix, and minor heavy minerals were deposited during sedimentation. IOH was first formed in early diagenesis, as recorded by those coating detrital grains along the dustlines and followed by quartz overgrowths, and then in later diagenetic stages together with quartz overgrowths, kaolinite, and illite. IOH was dissolved during bleaching, which mainly took place in late diagenesis when the sandstones were well compacted and cemented. Quartz overgrowths may have started development in early diagenesis, after the early IOH formation, and continued to form with increasing burial. At least one quartz dissolution event took place after the development of quartz overgrowths. Kaolinite was formed from early to late (as dickite) diagenesis, and was generally earlier than illite formation. Illite and associated APS precipitation partly overlaps with quartz overgrowth development and bleaching (removal of IOH), based on the observation that both illite and quartz overgrowth are better developed in bleached sandstones than the redbed counterparts (Chu et al., 2015), and outlasts all other diagenetic minerals.

6. Fluid inclusion microthermometry

Fluid inclusions are generally poorly developed in quartz overgrowths in the samples examined. Nevertheless, a total of 342 workable fluid inclusions were found in quartz overgrowths in different formations from the three drill cores (Table 1; Fig. 2). More workable fluid inclusions were found in the BL-08-01 drill core (n = 180) than in WC-79-1 (n = 98) and DV10-001 (n = 64). For BL-08-01, workable fluid inclusions were found in all the formations, i.e., from top to bottom, the Wolverine Point, Lazenby Lake, Manitou Falls, and Read formations (Fig. 2); for DV-10-001, which penetrates the Wolverine Point, Lazenby Lake, and Manitou Falls formations (Fig. 2), workable fluid inclusions were mostly seen in the lower two formations, whereas for WC-79-1, which penetrates the Lazenby Lake, Manitou Falls, and Read formations, workable inclusions were only found in the Manitou Falls Formation, the other two formations being very thin (Fig. 2).

Most fluid inclusions in quartz overgrowths are liquid-dominated biphase inclusions (Fig. 6a-e), with the vapor percentage being generally <15%. A few fluid inclusions containing a halite crystal (Fig. 6f) were also seen. Workable fluid inclusions are mostly 8–12 μm in size. The fluid inclusions are distributed along or near the dustlines (Fig. 6a, d and f), or are isolated (Fig. 6b and c) or clustered (Fig. 6e) within quartz overgrowths. There are commonly a number of fluid inclusions along

the same dustline, however, only a few of them are workable. The inclusions along the dustlines and the isolated inclusions are considered to be primary, and those in clusters or short trails within quartz overgrowths are likely pseudo-secondary. The fluid inclusion assemblage (FIA) concept (Goldstein and Reynolds, 1994) was applied to verify the validity of the microthermometric data, thus the variation of the homogenization temperatures of neighboring fluid inclusions in the same group (a dustline or a cluster) are limited to <15 °C, beyond which the fluid inclusions are considered to have experienced post-trapping stretching and the entire FIAs were eliminated. For isolated fluid inclusions, the FIA method cannot be strictly applied, but comparison of microthermometric data between neighboring inclusions was still made to minimize the adoption of fluid inclusions that may have been potentially stretched (Chi and Lu, 2008).

Homogenization temperatures (T_h) of all the fluid inclusions analyzed range from 50° to 235 °C (Table 1; Fig. 7), mainly from 60° to 180 °C. For the WC-79-1 drill core, the T_h values are all higher than 100 °C (103°–192 °C) in the upper part of the Manitou Falls Formation, and range from 50° to 218 °C in the lower part (Table 1; Fig. 7a). In contrast, for BL-08-01, the T_h values in the upper part of the drill core (the Wolverine Point Formation, Lazenby Lake Formation, and upper Manitou Falls Formation) fall in a range from 50° to 199 °C, whereas those from the lower Manitou Falls Formation and Read Formation are more scattered and range from 70° to 235 °C (Table 1; Fig. 7b). For the DV10-001 drill core, relatively low T_h values were obtained for all the formations, ranging from 65° to 202 °C (Table 1; Fig. 7c).

Ice-melting temperatures ($T_{m\text{-}ice}$) were measured for one-third of the biphase inclusions that have been measured for homogenization temperatures, the other two-thirds being either unable to freeze (after cooling to −185 °C) or too small for accurate measurement. Overall, the $T_{m\text{-}ice}$ values range from −9.2° to −48.6 °C, the majority being lower than the eutectic temperature of the H_2O-NaCl system (−21.2 °C) (Table 1). Assuming a H_2O-NaCl system for the fluid inclusions with $T_{m\text{-}ice} > -21.2$ °C and a H_2O–NaCl–$CaCl_2$ system for those with $T_{m\text{-}ice} < -21.2$ °C, the salinities were estimated to be from 13.1 to 30.7 wt.%. Six halite-bearing inclusions were observed in these three drill cores. Their halite-melting temperatures ($T_{m\text{-}halite}$) range from 141° to 218 °C, which are higher than the corresponding homogenization temperatures, and salinities were calculated from 31.0 to 32.9 wt.% (Table 1). Similar to the homogenization temperature distribution, no systematic variation of salinities with depth can be discerned (Fig. 8).

7. Illite geothermometry

A total of 121 pore-filling illite crystals (35 from WC-79-1, 34 from BL-08-01, and 52 from DV10-001; Fig. 2) were selected for electron microprobe analysis for major element compositions, which were used to calculate the formation temperatures. Pore-filling rather than replacement illite was analyzed in order to minimize the influence of precursor minerals, and isolated crystals were chosen for analysis to avoid contamination from neighboring minerals.

The EMPA results (Table 2) indicate that the major constituents SiO_2, Al_2O_3, FeO, MgO, CaO, Na_2O, and K_2O account for 70–94 wt.% in total (Table 2). These results were normalized to 100% and used to calculate site occupancy and fractions of end-member minerals (Table 2). No systematic differences in illite composition can be discerned between samples from different locations (Table 2).

The formation temperatures of illite were calculated using the site occupancy and end-member mineral data (Table 2) and the equations of Cathelineau (1988)'s and Battaglia (2004). The calculation results are shown in Table 2 and illustrated in Fig. 9. For the WC-79-1 drill core, calculated temperatures mainly range from 220° to 260 °C (Table 2; Fig. 9a and d). The highest values are located at 339 m and the lowest value at 425 m (Fig. 9a and d). For the BL-08-01 drill core, the calculated temperatures mainly range from 230° to 270 °C, with the lowest in the Lazenby Lake Formation and highest in the bottom of Manitou Falls Formation (Table 2; Fig. 9b and e). For the DV10-001 drill core, the calculated temperatures mainly range from 240° to 280 °C using the equations of Cathelineau (1988) and from 240° to 260 °C with those of Battaglia (2004) (Table 2; Fig. 9c and f).

Overall, illite crystallization temperatures calculated using the equations of Cathelineau (1988) range from 212° to 298 °C, and using Battaglia (2004)'s method range from 228° to 298 °C (Table 2). The discrepancies between the two methods for individual samples are generally within 10 °C. No obvious trends can be discerned in the temperature-depth diagrams for each drill core, and there is no significant difference between drill cores. In comparison with fluid inclusion homogenization temperatures, the calculated illite crystallization temperatures using the methods of both Cathelineau (1988) and Battaglia (2004) are systematically higher (with limited overlap) (Table 2; Fig. 10).

8. Discussion

A few notable characteristics of the fluid inclusion and illite geothermometric study results emerge from this study. Firstly, homogenization temperatures of fluid inclusions from quartz overgrowths cover a wide range at any given depth, and they do not show a systematic increase with depth (Fig. 7). Secondly, the calculated illite crystallization temperatures are systematically higher than the fluid inclusion homogenization temperatures, and they do not show an obvious trend of increase with depth either (Figs. 9 and 10). Thirdly, the ice-melting temperatures of fluid inclusions are mostly lower than −21.2 °C (the eutectic point for the H_2O–NaCl system), suggesting that the fluids may be approximated by the H_2O–NaCl–$CaCl_2$ system, and there is no systematic change of fluid salinities with depth (Fig. 8). Finally, there are no systematic differences in fluid inclusion homogenization temperatures, illite crystallization temperatures, and fluid compositions between the studied drill cores from different parts of the Athabasca Basin (Fig. 10). The significance and implications of these basin-scale fluid characteristics for basinal fluid flow and uranium mineralization are discussed below.

8.1. Range of fluid inclusion homogenization temperatures

The wide range of homogenization temperatures of fluid inclusions within quartz overgrowths documented in this study, mainly from 60° to 180 °C (Table 1 and Fig. 7), is interpreted to indicate that the quartz overgrowths were precipitated over a wide range of thermal conditions during the long diagenetic history of the Athabasca basin, as is common in many sedimentary basins (e.g., Chi et al., 2003; Hiemstra and Goldstein, 2005). The application of the fluid inclusion assemblage concept (Goldstein and Reynolds, 1994) suggests that the variation of fluid inclusion homogenization temperatures within individual quartz overgrowths is not a result of post-trapping modification of the fluid inclusions; post-trapping modification would result in variation of homogenization temperatures within individual fluid inclusion assemblages, in which case the data were rejected. Similar ranges of homogenization temperatures have also been reported in previous studies of fluid inclusions in quartz overgrowths in the Athabasca basin (Pagel, 1975; Kotzer and Kyser, 1995; Scott and Chi, 2014), although the homogenization temperature values of Pagel (1975) are relatively low compared to those of other studies. The interpretation of quartz cementation over a wide range of thermal conditions is also consistent with the wide range of oxygen isotope data of quartz overgrowths from the Athabasca basin (Hiatt et al., 2007). For sedimentary basins with a simple burial history, it may be expected that the part of quartz overgrowth close to the dustline was precipitated at a relatively shallow and cool environment, whereas the part filling the center of the interstitial space was formed in a relatively deep and hot environment. However, for a basin with a complex burial and uplifting

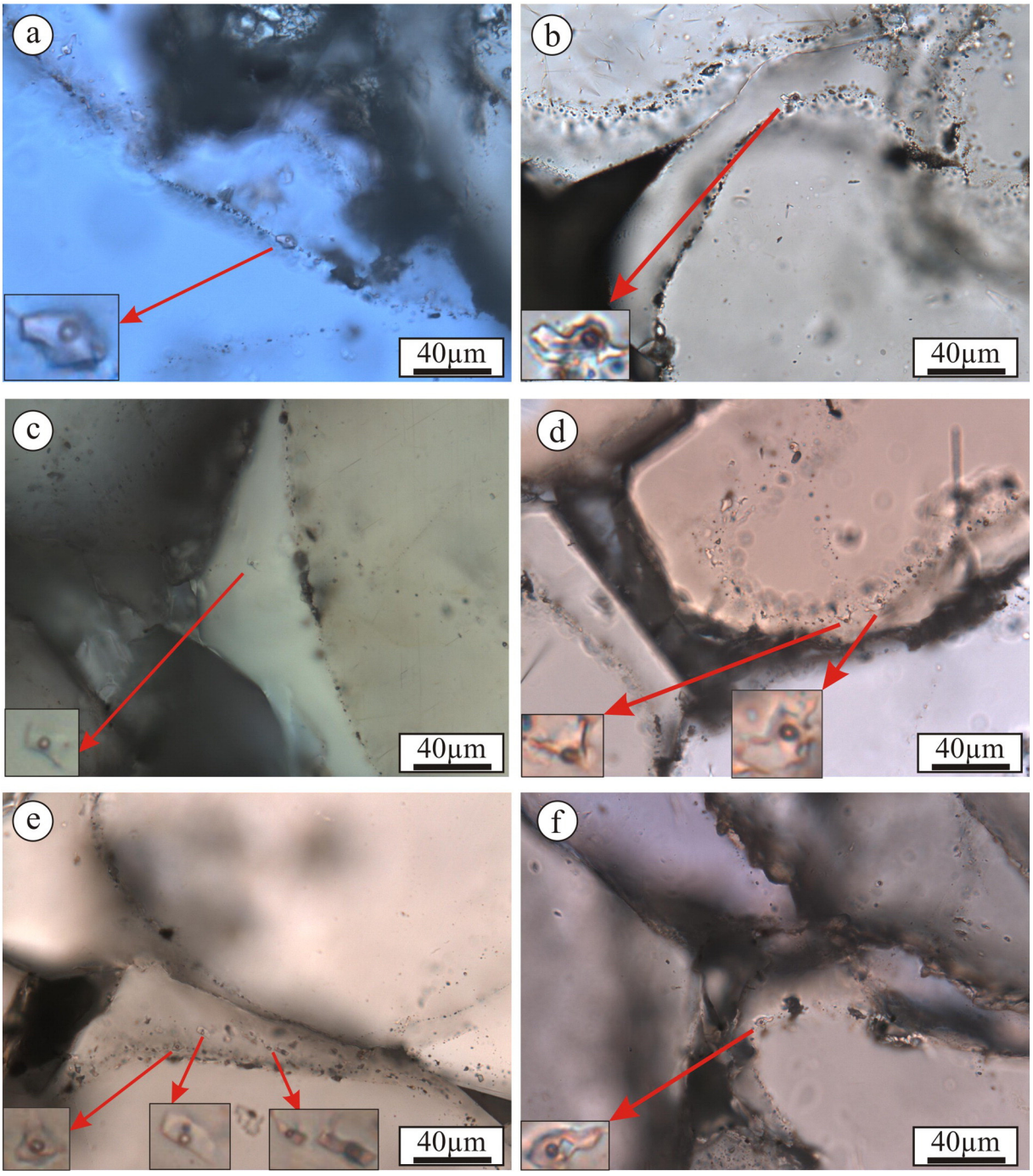

Fig. 6. Photomicrographs of different types of fluid inclusions in quartz overgrowths (all in plane polarized light). a — L–V (liquid–vapor) fluid inclusions along the dustline, sample 1454 from BL-08-01 drill core; b — a L–V fluid inclusion near the dustline in the quartz overgrowth, sample 1422 from WC-79-1 drill core; c — an isolated L–V fluid inclusion in quartz overgrowth away from the dustline, sample 1337 from DV10-001 drill core; d —L–V fluid inclusions along the dustline, sample 1436 from WC-79-1 drill core; e — L-V fluid inclusion trails in quartz overgrowth, sample 1404 from WC-79-1 drill core; f — a halite-bearing fluid inclusion along the dustline, sample 1442 from BL-08-01 drill core.

history like the Athabasca basin, such a regular thermal pattern may not be seen. In fact, many of the fluid inclusions close to the dustline have fairly high homogenization temperatures, suggesting that quartz overgrowths do not necessarily start precipitation at shallow burial. Conversely, some fluid inclusions away from the dustline show relatively low homogenization temperatures, suggesting that the late phase of quartz overgrowth was not necessarily formed at higher temperatures than the early phase. Overall, the range of homogenization temperatures of fluid inclusions in quartz overgrowths reflects the range of thermal conditions that the strata experienced, and the maximum homogenization temperatures do not necessarily represent the maximum burial conditions.

8.2. Difference between fluid inclusion homogenization temperatures and calculated illite temperatures

The observation that illite crystallization temperatures (mainly from 220° to 270 °C) are higher than the fluid inclusion homogenization temperatures (mainly from 60° to 180 °C) (Fig. 10) may be attributed to the fact that fluid inclusion homogenization temperatures only represent

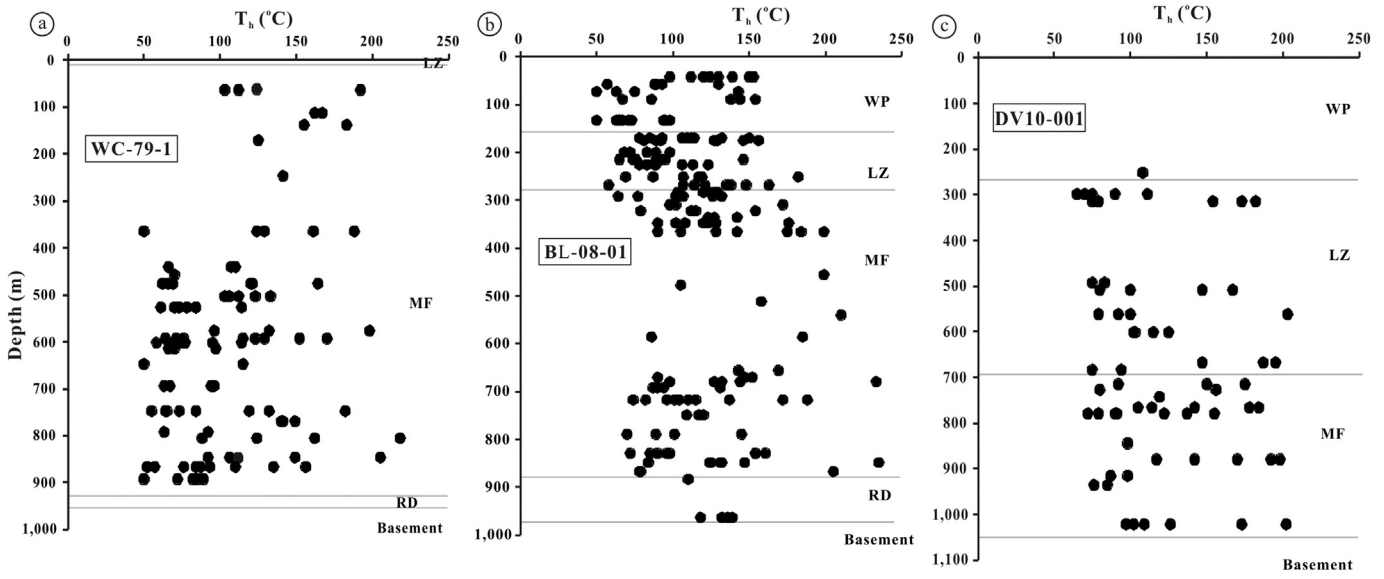

Fig. 7. Distribution of fluid inclusion homogenization temperatures along depth from the WC-79-1, BL-08-01, and DV10-001 drill cores.

the minimum trapping temperatures and that illite was not co-precipitated with quartz overgrowths. Furthermore, different types of illite have been reported in the Athabasca basin, and the illite examined in this study may not cover all the types.

It is well known that the homogenization temperatures of fluid inclusions are generally lower than the trapping temperatures except in the cases of fluid boiling or immiscibility (Roedder, 1984). No evidence of fluid boiling or immiscibility has been found in our study, and therefore the homogenization temperatures need to be "pressure-corrected" in order to obtain the trapping temperatures. To make this correction, the fluid pressures need to be independently determined, and the isochores of the fluid inclusions need to be constructed. The isochores were calculated with the computer program 'FLUIDS 1' of Bakker (2003): the bulk fluid density was first calculated with the 'BULK' program, using the empirical equations of state of Oakes et al. (1990) and Zhang and Frantz (1987), and then used to calculate the isochores with the 'ISOC' program, using the empirical equations of state of Bodnar and Vityk (1994) and Knight and Bodnar (1989) as implemented in the computer programs (Bakker, 2003). Although there are significant uncertainties about the thickness of sedimentary rocks that have been eroded above the currently preserved strata, the erosion is likely less than 5 km (Pagel, 1975). Assuming a maximum erosion of 5 km and a hydrostatic pressure regime (Chi et al., 2013), and applying the fluid pressures to the isochores, it was found that maximum temperature correction is only 31 °C. Even if this temperature is added to all the homogenization temperatures, the resulting "pressure-corrected" temperatures are still lower than the illite temperatures, as can be seen from Fig. 10.

As discussed above, the wide range of fluid inclusion homogenization temperatures reflects variable thermal conditions in which the quartz overgrowths were formed, and the maximum homogenization temperatures, even after pressure correction, do not necessarily represent the maximum thermal conditions. In fact, petrographic studies indicate that illite precipitation partly overlaps with, and generally postdates,

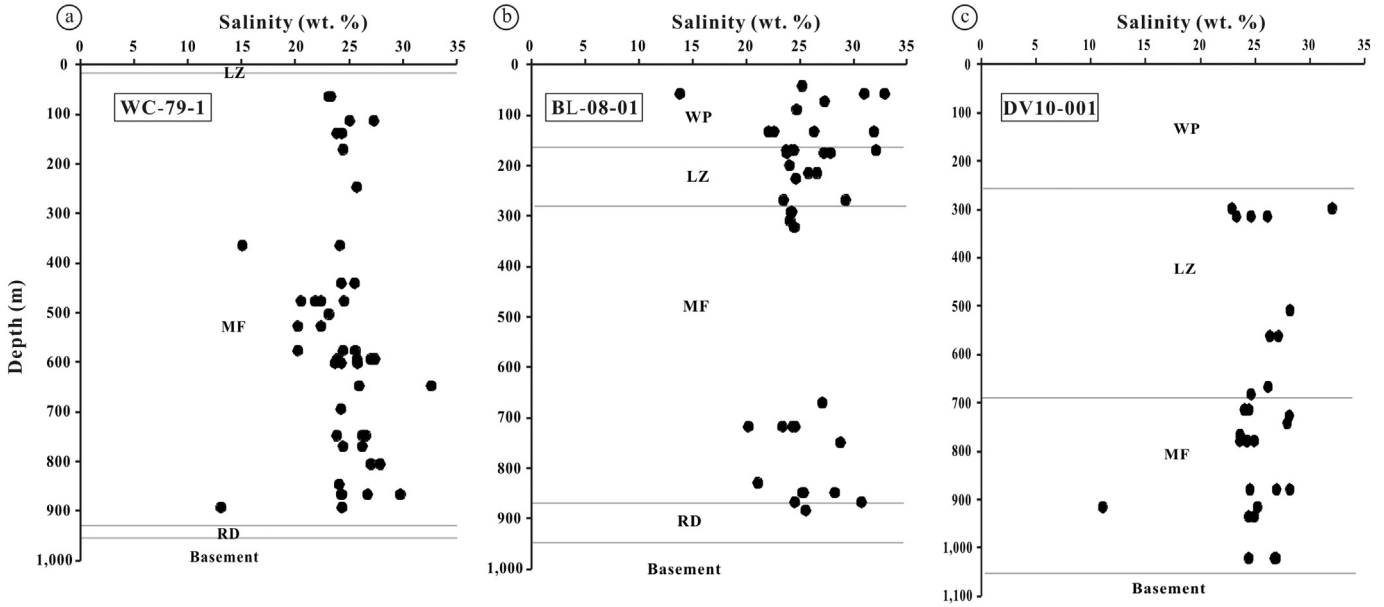

Fig. 8. Distribution of salinities of fluid inclusions along depth of the WC-79-1, BL-08-01, and DV10-001 drill cores.

Table 2
EMPA results and calculated crystallization temperatures of illite from sandstones in the Athabasca basin.

Sample #	Depth (m)	Point #	Oxide Weight%								Site Occupancy										End Members						T1* (°C)	Ave1 (°C)	σ1 (°C)	T2* (°C)	Ave2 (°C)	σ2 (°C)
			SiO_2	Al_2O_3	FeO	MgO	CaO	Na_2O	K_2O	Total	K	Na	Ca	IC	Si(IV)	Al(IV)	Al(VI)	Fe	Mg	R^{2+}	Fe-cel.	Mg-cel.	Par.	Ca-par.	Mus.	Pyr.						
WC-79-1 drill core																																
1407	138.0	1	38.98	24.44	0.67	0.69	0.22	0.15	6.90	72.05	0.76	0.03	0.02	0.82	3.36	0.64	1.85	0.05	0.09	0.14	0.05	0.09	0.03	0.04	0.62	0.18	247	235	18	246	237	13
		4	37.88	24.87	0.65	0.71	0.26	0.16	6.15	70.68	0.69	0.03	0.02	0.76	3.32	0.68	1.88	0.05	0.09	0.14	0.05	0.09	0.03	0.05	0.55	0.24	222			228		
1411	254.5	1	37.51	25.58	1.88	0.73	0.14	0.32	6.85	73.01	0.75	0.05	0.01	0.83	3.23	0.77	1.83	0.14	0.09	0.23	0.14	0.09	0.05	0.03	0.52	0.17	250	238	16	244	240	11
		3	39.27	26.17	1.21	0.68	0.08	0.20	6.89	74.50	0.74	0.03	0.01	0.78	3.28	0.72	1.86	0.08	0.08	0.17	0.08	0.08	0.03	0.01	0.57	0.22	230			229		
		6	43.45	30.23	1.20	0.94	0.15	0.12	8.46	84.55	0.80	0.02	0.01	0.84	3.22	0.78	1.86	0.07	0.10	0.18	0.07	0.10	0.02	0.02	0.62	0.16	253			254		
		7	45.73	31.39	1.05	0.97	0.12	0.14	7.91	87.31	0.72	0.02	0.01	0.76	3.25	0.75	1.89	0.06	0.10	0.17	0.06	0.10	0.02	0.02	0.55	0.24	219			235		
1412	281.2	1	39.44	26.97	0.84	0.77	0.14	0.11	7.11	75.38	0.75	0.02	0.01	0.79	3.26	0.74	1.88	0.06	0.09	0.15	0.06	0.09	0.02	0.02	0.60	0.21	234			242		
		3	42.29	28.56	0.89	1.07	0.20	0.11	7.97	81.09	0.78	0.02	0.02	0.83	3.26	0.74	1.85	0.06	0.12	0.18	0.06	0.12	0.02	0.03	0.60	0.17	250	248	14	259	255	12
		7	36.24	25.54	0.7	1.01	0.21	0.17	7.02	70.89	0.79	0.03	0.02	0.86	3.20	0.80	1.86	0.05	0.13	0.18	0.05	0.13	0.03	0.04	0.61	0.14	261			265		
1414	318.2	a	37.72	25.53	1.33	0.78	0.11	0.26	6.63	72.36	0.73	0.04	0.01	0.79	3.26	0.74	1.85	0.10	0.10	0.20	0.10	0.10	0.04	0.02	0.53	0.21	235			228		
		b1	38.31	25.63	0.70	0.87	0.44	0.19	6.51	72.65	0.71	0.03	0.04	0.82	3.28	0.72	1.86	0.05	0.11	0.16	0.05	0.11	0.03	0.08	0.55	0.18	246	245	23	238	245	19
		b2	38.76	25.76	0.72	0.72	0.19	0.11	6.47	72.73	0.70	0.02	0.02	0.76	3.30	0.70	1.89	0.05	0.09	0.14	0.05	0.09	0.02	0.03	0.56	0.24	219			231		
1415	338.5	2	37.40	25.75	0.77	0.84	0.19	0.14	7.77	72.86	0.86	0.02	0.02	0.91	3.23	0.77	1.84	0.06	0.11	0.16	0.06	0.11	0.02	0.04	0.69	0.09	283	261	30	275	264	14
		3	38.52	24.03	0.68	1.04	0.21	0.13	6.11	70.72	0.75	0.02	0.02	0.81	3.36	0.64	1.82	0.05	0.14	0.18	0.05	0.14	0.02	0.04	0.56	0.19	214			254		
1417	391.2	1	39.05	24.48	0.95	1.40	0.16	0.16	7.33	73.53	0.80	0.03	0.01	0.85	3.32	0.68	1.78	0.07	0.18	0.25	0.07	0.18	0.03	0.03	0.55	0.15	258			274		
		2	44.34	29.19	0.59	0.97	0.09	0.11	7.83	83.12	0.75	0.02	0.01	0.78	3.31	0.69	1.88	0.04	0.11	0.14	0.04	0.11	0.02	0.01	0.60	0.22	227	251	21	250	261	12
		6	37.32	25.72	0.69	0.76	0.30	0.13	7.25	72.17	0.80	0.02	0.03	0.88	3.24	0.76	1.86	0.05	0.10	0.15	0.05	0.10	0.02	0.06	0.65	0.12	269			259		
1418	424.8	a1	39.83	22.96	0.87	0.96	0.19	0.17	5.98	70.96	0.66	0.03	0.02	0.73	3.46	0.54	1.81	0.06	0.12	0.19	0.06	0.12	0.03	0.04	0.48	0.27	208	224	22	225	240	20
		a2	38.09	23.47	0.67	0.94	0.16	0.12	6.68	70.13	0.75	0.02	0.02	0.81	3.37	0.63	1.82	0.05	0.12	0.17	0.05	0.12	0.02	0.03	0.58	0.19	239			254		
1425	576.5	1	38.37	24.09	0.92	0.71	0.24	0.12	6.80	71.25	0.76	0.02	0.02	0.82	3.35	0.65	1.83	0.07	0.09	0.16	0.07	0.09	0.02	0.04	0.60	0.18	246	240	9	241	242	1
		2	37.88	24.74	0.70	0.67	0.13	0.10	6.72	70.94	0.75	0.02	0.01	0.79	3.32	0.68	1.87	0.05	0.09	0.14	0.05	0.09	0.02	0.02	0.61	0.21	234			242		
1427	601.2	5	37.84	26.07	0.81	0.75	0.13	0.14	7.18	72.92	0.78	0.02	0.01	0.83	3.24	0.76	1.87	0.06	0.10	0.15	0.06	0.10	0.02	0.02	0.63	0.17	250	236	19	252	240	16
		7	37.56	26.13	0.58	0.62	0.19	0.18	6.32	71.58	0.70	0.03	0.02	0.76	3.25	0.75	1.91	0.04	0.08	0.12	0.04	0.08	0.03	0.04	0.58	0.24	222			229		
1439	911.7	a1	44.92	32.72	0.56	0.59	0.13	0.11	8.54	87.57	0.77	0.02	0.01	0.81	3.19	0.81	1.94	0.03	0.06	0.10	0.03	0.06	0.02	0.02	0.68	0.19	241			247		
		a2	43.84	32.21	0.58	0.59	0.12	0.10	8.07	85.51	0.75	0.01	0.01	0.78	3.19	0.81	1.94	0.04	0.06	0.10	0.04	0.06	0.01	0.02	0.65	0.22	229			240		
		b1	41.85	31.15	0.47	0.45	0.07	0.12	8.01	82.12	0.77	0.02	0.01	0.80	3.17	0.83	1.95	0.03	0.05	0.08	0.03	0.05	0.02	0.01	0.69	0.20	238	241	6	245	248	5
		b2	41.84	30.33	0.73	0.59	0.07	0.08	8.13	81.77	0.79	0.01	0.01	0.81	3.19	0.81	1.92	0.05	0.07	0.11	0.05	0.07	0.01	0.01	0.68	0.19	243			249		
		b3	42.81	31.91	0.53	0.59	0.09	0.09	8.40	84.42	0.79	0.01	0.01	0.82	3.16	0.84	1.94	0.03	0.06	0.10	0.03	0.06	0.01	0.01	0.69	0.18	245			252		
		b4	42.53	31.27	0.61	0.55	0.08	0.07	8.44	83.55	0.80	0.01	0.01	0.83	3.18	0.82	1.93	0.04	0.06	0.10	0.04	0.06	0.01	0.01	0.71	0.17	248			253		
1440	930.7	c	42.33	31.39	0.62	0.58	0.13	0.09	8.18	83.32	0.78	0.01	0.01	0.81	3.17	0.83	1.94	0.04	0.06	0.10	0.04	0.06	0.01	0.02	0.68	0.19	243			248		
		d	42.63	31.6	0.55	0.48	0.07	0.05	7.90	83.28	0.75	0.01	0.01	0.77	3.18	0.82	1.96	0.03	0.05	0.09	0.03	0.05	0.01	0.01	0.66	0.23	225			238		
		e1	45.16	32.93	0.58	0.52	0.10	0.08	8.66	88.03	0.78	0.01	0.01	0.81	3.19	0.81	1.94	0.03	0.05	0.09	0.03	0.05	0.01	0.02	0.69	0.19	240	238	12	246	246	7
		e2	46.69	34.47	0.6	0.52	0.08	0.06	9.22	91.64	0.80	0.01	0.01	0.82	3.18	0.82	1.94	0.03	0.05	0.09	0.03	0.05	0.01	0.01	0.71	0.18	245			251		
		e3	45.83	33.83	0.53	0.54	0.07	0.07	8.35	89.22	0.74	0.01	0.01	0.76	3.19	0.81	1.96	0.03	0.06	0.09	0.03	0.06	0.01	0.01	0.65	0.24	221			237		
		e4	45.25	32.98	0.61	0.70	0.13	0.11	8.91	88.69	0.80	0.02	0.01	0.83	3.18	0.82	1.92	0.04	0.07	0.11	0.04	0.07	0.02	0.02	0.69	0.17	251			256		
BL-08-01 drill core																																
1446	132.0	a1	40.27	29.62	0.70	0.48	0.16	0.11	8.24	79.58	0.83	0.02	0.01	0.87	3.17	0.83	1.92	0.05	0.06	0.10	0.05	0.06	0.02	0.03	0.72	0.13	266			256		
		a2	43.67	31.90	0.84	0.51	0.16	0.10	8.10	85.28	0.75	0.01	0.01	0.79	3.19	0.81	1.93	0.05	0.06	0.11	0.05	0.06	0.01	0.03	0.65	0.21	235	252	16	235	246	11
		b1	40.77	29.05	1.75	0.8	0.25	0.13	7.89	80.64	0.79	0.02	0.02	0.85	3.18	0.82	1.85	0.11	0.09	0.21	0.11	0.09	0.02	0.04	0.58	0.15	256			248		
1449	199.3	a1	43.17	30.64	0.62	0.53	0.10	0.11	8.12	83.29	0.77	0.02	0.01	0.81	3.23	0.77	1.92	0.04	0.06	0.10	0.04	0.06	0.02	0.02	0.68	0.19	239			244		
		a2	42.97	20.35	0.57	0.42	0.30	0.21	5.86	70.68	0.65	0.04	0.03	0.74	3.71	0.29	1.79	0.04	0.05	0.10	0.04	0.05	0.04	0.06	0.55	0.26	212	239	27	208	236	25
		b	39.45	28.49	1.15	0.67	0.14	0.08	8.11	78.09	0.83	0.01	0.01	0.87	3.18	0.82	1.88	0.08	0.08	0.16	0.08	0.08	0.01	0.02	0.68	0.13	265			255		
1450	214.5	1	37.16	27.40	0.66	0.53	0.21	0.12	7.44	73.52	0.81	0.02	0.02	0.87	3.16	0.84	1.91	0.05	0.07	0.11	0.05	0.07	0.02	0.04	0.69	0.13	264	266	4	253	256	4
		7	34.88	26.48	0.97	0.54	0.08	0.08	7.46	70.49	0.85	0.01	0.01	0.88	3.12	0.88	1.91	0.07	0.07	0.14	0.07	0.07	0.01	0.02	0.71	0.12	269			259		
1451	225.4	3	45.31	30.81	0.86	0.59	0.15	0.11	8.80	86.63	0.81	0.02	0.01	0.85	3.27	0.73	1.88	0.05	0.06	0.12	0.05	0.06	0.02	0.02	0.69	0.15	256	268	17	251	258	10
		4	37.90	28.05	0.74	0.47	0.10	0.14	8.16	75.56	0.87	0.02	0.01	0.91	3.15	0.85	1.91	0.05	0.06	0.11	0.05	0.06	0.02	0.02	0.76	0.09	280			265		
1452	250.8	1	38.23	29.25	0.59	0.71	0.09	0.12	7.89	76.88	0.82	0.02	0.01	0.85	3.12	0.88	1.93	0.04	0.09	0.13	0.04	0.09	0.02	0.02	0.69	0.15	259			264		
		2	41.01	29.66	0.63	0.72	0.12	0.15	7.70	79.99	0.76	0.02	0.01	0.81	3.19	0.81	1.92	0.04	0.08	0.12	0.04	0.08	0.02	0.02	0.64	0.19	240	253	11	248	255	8
		4	41.94	30.17	0.66	0.52	0.17	0.07	8.37	81.90	0.81	0.01	0.01	0.85	3.20	0.80	1.91	0.04	0.06	0.10	0.04	0.06	0.01	0.03	0.71	0.15	258			254		
1453	267.7	4	41.50	30.53	0.61	0.62	0.13	0.08	8.48	81.95	0.83	0.01	0.01	0.86	3.17	0.83	1.92	0.04	0.07	0.11	0.04	0.07	0.01	0.02	0.72	0.14	261	261	0	261	261	0
1457	321.6	1	41.21	29.18	0.43	0.00	0.10	0.08	7.14	78.14	0.72	0.01	0.01	0.75	3.26	0.74	1.98	0.03	0.00	0.03	0.03	0.00	0.01	0.02	0.69	0.25	217	221	6	232	237	7
		3	41.10	29.49	0.54	0.01	0.09	0.05	7.46	78.74	0.75	0.01	0.01	0.77	3.24	0.76	1.97	0.04	0.00	0.04	0.04	0.00	0.01	0.02	0.71	0.23	226			241		
1460	365.1	1	39.51	27.54	0.72	0.00	0.10	0.09	7.79	75.75	0.82	0.01	0.01	0.85	3.26	0.74	1.93	0.05	0.00	0.05	0.05	0.00	0.01	0.02	0.77	0.15	258	255	3	264	263	2
		3	35.75	25.17	0.72	0.00	0.10	0.11	6.93	68.78	0.80	0.02	0.01	0.84	3.24	0.76	1.94	0.05	0.00	0.05	0.05	0.00	0.02	0.02	0.75	0.16	253			261		
1469	655.4	a1	40.83	29.02	0.71	1.07	0.24	0.07	7.79	79.73	0.78	0.01	0.02	0.83	3.20	0.80	1.88	0.05	0.12	0.17	0.05	0.12	0.01	0.04	0.61	0.17	249			261		
		a2	39.15	27.61	0.58	0.62	0.19	0.06	7.85	76.06	0.82	0.01	0.02	0.87	3.22	0.78	1.89	0.04	0.08	0.12	0.04	0.08	0.01	0.03	0.71	0.13	264	249	11	262	256	7
		b1	47.10	33.82	0.68	0.69	0.12	0.06	9.12	91.59	0.79	0.01	0.01	0.82	3.21	0.79	1.92	0.04	0.07	0.11	0.04	0.07	0.01	0.02	0.68	0.18	244			252		
		b2	42.11	29.59	0.57	0.76	0.17	0.11	7.77	81.08	0.76	0.02	0.01	0.80	3.23	0.77	1.91	0.04	0.09	0.12	0.04	0.09	0.02	0.03	0.64	0.20	239			249		
1475	768.1	2	37.46	27.19	0.69	0.00	0.25	0.06	6.80	72.45	0.74	0.01	0.02	0.80	3.21	0.79	1.96	0.05	0.00	0.05	0.05	0.00	0.01	0.05	0.69	0.20	237	262	18	244	261	11
		3	42.17	31.43	0.61	0.00	0.13	0.06	8.90	83.30	0.85	0.01	0.01	0.88	3.17	0.83	1.96	0.04	0.00	0.04	0.04	0.00	0.01	0.02	0.82	0.12	270			271		
		4	42.66	30.95	0.62	0.00	0.14	0.09	8.59	83.05	0.82	0.01	0.01	0.86	3.21	0.79	1.95	0.04	0.00	0.04	0.04	0.00	0.01	0.02	0.79	0.14	261			263		
		5	38.63	28.89	0.77	0.00	0.32	0.17	7.86	76.64	0.82	0.03	0.03	0.90	3.16	0.84	1.94	0.05	0.00	0.05	0.05	0.00	0.03	0.06	0.77	0.10	278			265		
1476	788.9	3	36.99	25.82	0.56	0.00	0.22	0.09	7.12	70.80	0.80	0.02	0.02	0.86	3.26	0.74	1.93	0.04	0.00	0.04	0.04	0.00	0.02	0.04	0.76	0.14	260	260	0	257	257	0
1477	828.4	6	38.61	25.58	0.57	0.00	0.60	0.07	6.65	72.08	0.73	0.01	0.06	0.85	3.32	0.68	1.91	0.04	0.00	0.04	0.04	0.00	0.01	0.11	0.69	0.15	258	247	15	238	239	1
		7	38.39	24.38	0.57	0.00	0.20	0.14	6.55	70.23	0.74	0.02	0.02	0.80	3.38	0.62	1.91	0.04	0.00	0.04	0.04	0.00	0.02	0.04	0.69	0.20	236			240		
1478	847.9	1	37.46	25.86	0.43	0.00	0.28	0.07	6.79	70.89	0.76	0.01	0.03	0.82	3.28	0.72	1.95	0.03	0.00	0.03	0.03	0.00	0.01	0.05	0.73	0.18	246	270	21	243	251	17
		3	37.94	28.07	0.62	0.00	0.31	0.18	8.15	75.27	0.87	0.03	0.03	0.95	3.17	0.83	1.93	0.04	0.00	0.04	0.04	0.00	0.03	0.06	0.82	0.05	298			276		
		6	36.46	26.51	0.42	0.00	0.72	0.06	6.56	70.73	0.74	0.01	0.07	0.88	3.20	0.80	1.95	0.03	0.00	0.03	0.03	0.00	0.01	0.14	0.70	0.12	270			237		
		7	39.68	28.90	0.44	0.00	0.44	0.12	7.58	77.16	0.78	0.02	0.04	0.88	3.20	0.80	1.95	0.03	0.00	0.03	0.03	0.00	0.02	0.08	0.75	0.12	267			249		
1479	866.6	5	37.02	27.98	0.55	0.00	0.24	0.07	7.22	73.08	0.79	0.01	0.02	0.84	3.16	0.84	1.97	0.04	0.00	0.04	0.04	0.00	0.01	0.04	0.75	0.16	254	254	0	253	253	0

formation of quartz overgrowths. Therefore, it is not surprising that illite was formed at higher temperatures than quartz overgrowths.

Previous studies of clay minerals in the Athabasca basin and unconformity-related uranium deposits have identified a lath-like/platy (1Mc, originally termed as 3T) illite and a fibrous/hairy (1Mt) illite (Hoeve and Quirt, 1984; Drits et al., 1993; Kotzer and Kyser, 1995; Laverret et al., 2006; Kister et al., 2005, 2006; Quirt, 2010). The 1Mc polytype has been considered to be of diagenetic origin, and the 1 Mt of hydrothermal origin (Laverret et al., 2006; Kister et al., 2005, 2006; Quirt, 2010). Kotzer and Kyser (1995) obtained temperatures of 140° to 240 °C from highly crytalline 2M/3T (1Mc?) illite, based on illite-kaolinite and illite-quartz oxygen isotope geothermometers, and

Sample #.	Depth (m)	Point #	Oxide Weight%								Site Occupancy										End Members						T1* (°C)	Ave1 (°C)	σ1 (°C)	T2* (°C	Ave2 (°C)	σ2 (°C)
			SiO_2	Al_2O_3	FeO	MgO	CaO	Na_2O	K_2O	Total	K	Na	Ca	IC	Si(IV)	Al(IV)	Al(VI)	Fe	Mg	R^{2+}	Fe-cel.	Mg-cel.	Par.	Ca-par.	Mus.	Pyr.						
DV10-001 drill core																																
1215	297.7	2	37.48	24.99	0.12	1.19	0.36	0.11	7.18	71.43	0.80	0.02	0.03	0.88	3.27	0.73	1.84	0.01	0.15	0.16	0.01	0.15	0.02	0.07	0.64	0.12	271			285		
		4	37.19	25.17	0.16	1.16	0.23	0.06	7.57	71.54	0.84	0.01	0.02	0.90	3.25	0.75	1.84	0.01	0.15	0.16	0.01	0.15	0.01	0.04	0.68	0.10	276			295		
		5	42.77	28.34	0.18	1.31	0.19	0.03	7.75	80.57	0.76	0.00	0.02	0.80	3.29	0.71	1.86	0.01	0.15	0.16	0.01	0.15	0.00	0.03	0.60	0.20	236	264	18	273	284	12
		6	38.56	26.68	0.18	1.21	0.26	0.02	8.05	74.96	0.86	0.00	0.02	0.91	3.22	0.78	1.85	0.01	0.15	0.16	0.01	0.15	0.00	0.05	0.69	0.09	280			298		
		8	36.42	25.21	0.22	0.95	0.33	0.03	6.94	70.10	0.79	0.01	0.03	0.85	3.24	0.76	1.88	0.02	0.13	0.14	0.02	0.13	0.01	0.06	0.64	0.15	259			272		
1218	365.2	1	43.30	29.51	0.78	0.00	0.17	0.05	7.96	81.77	0.77	0.01	0.01	0.81	3.29	0.71	1.93	0.05	0.00	0.05	0.05	0.00	0.01	0.03	0.72	0.19	240			252		
		2	47.80	32.30	0.94	0.00	0.14	0.11	8.46	89.75	0.75	0.01	0.01	0.78	3.30	0.70	1.94	0.05	0.00	0.05	0.05	0.00	0.01	0.02	0.69	0.22	230	241	11	246	252	5
		3	42.35	29.28	0.89	0.00	0.26	0.12	8.00	80.90	0.79	0.02	0.02	0.85	3.26	0.74	1.92	0.06	0.00	0.06	0.06	0.00	0.02	0.04	0.73	0.15	256			258		
		4	46.68	32.71	0.90	0.00	0.14	0.07	8.78	89.28	0.78	0.01	0.01	0.81	3.25	0.75	1.94	0.05	0.00	0.05	0.05	0.00	0.01	0.02	0.73	0.19	242			255		
1226	520.1	2	47.04	33.59	0.72	0.72	0.09	0.05	9.03	91.24	0.79	0.01	0.01	0.81	3.21	0.79	1.92	0.04	0.07	0.11	0.04	0.07	0.01	0.01	0.67	0.19	240			251		
		3	43.99	30.74	0.87	0.63	0.17	0.07	8.73	85.20	0.82	0.01	0.01	0.85	3.23	0.77	1.89	0.05	0.07	0.12	0.05	0.07	0.01	0.03	0.70	0.15	259	262	21	255	262	14
		4	37.86	26.96	0.73	0.70	0.14	0.06	8.37	74.82	0.90	0.01	0.01	0.93	3.19	0.81	1.87	0.05	0.09	0.14	0.05	0.09	0.01	0.03	0.76	0.07	291			282		
		6	40.66	29.20	0.76	0.67	0.14	0.06	8.18	79.67	0.82	0.01	0.01	0.85	3.19	0.81	1.90	0.05	0.08	0.13	0.05	0.08	0.01	0.02	0.69	0.15	258			259		
1233	641.6	1	45.50	32.82	0.87	1.24	0.33	0.13	8.79	89.68	0.78	0.02	0.02	0.85	3.17	0.83	1.87	0.05	0.13	0.18	0.05	0.13	0.02	0.05	0.60	0.15	257			262		
		3	44.42	31.65	0.98	0.75	0.11	0.07	9.16	87.14	0.84	0.01	0.01	0.87	3.20	0.80	1.88	0.06	0.08	0.14	0.06	0.08	0.01	0.02	0.70	0.13	264	258	10	263	261	7
		4	44.35	32.04	0.77	0.74	0.10	0.06	9.26	87.32	0.85	0.01	0.01	0.87	3.19	0.81	1.90	0.05	0.08	0.13	0.05	0.08	0.01	0.02	0.72	0.13	266			268		
		5	45.62	32.52	0.98	0.8	0.10	0.05	8.85	88.92	0.79	0.01	0.01	0.82	3.21	0.79	1.90	0.06	0.08	0.14	0.06	0.08	0.01	0.02	0.65	0.18	243			251		
1242	795.2	1	39.65	26.31	0.67	0.87	0.51	0.23	7.40	75.64	0.78	0.04	0.05	0.91	3.28	0.72	1.84	0.05	0.11	0.15	0.05	0.11	0.04	0.09	0.63	0.09	280			257		
		2	41.42	28.49	0.70	0.81	0.34	0.18	8.25	80.19	0.82	0.03	0.03	0.91	3.24	0.76	1.86	0.05	0.09	0.14	0.05	0.09	0.03	0.06	0.68	0.09	280	278	3	265	269	15
		3	38.38	25.74	0.74	1.07	0.09	0.05	8.03	74.10	0.87	0.01	0.01	0.89	3.25	0.75	1.83	0.05	0.14	0.19	0.05	0.14	0.01	0.02	0.68	0.11	274			286		
1245	860.9	3	38.00	28.19	0.63	0.36	0.09	0.02	7.88	75.17	0.84	0.00	0.01	0.86	3.17	0.83	1.93	0.04	0.04	0.09	0.04	0.04	0.00	0.02	0.75	0.14	260	264	6	256	259	4
		4	38.91	27.62	0.57	0.38	0.10	0.05	8.06	75.69	0.85	0.01	0.01	0.88	3.22	0.78	1.91	0.04	0.05	0.09	0.04	0.05	0.01	0.02	0.76	0.12	268			261		
1246	878.7	2	47.02	31.29	1.41	1.53	0.10	0.07	9.44	90.86	0.83	0.01	0.01	0.86	3.25	0.75	1.80	0.08	0.16	0.24	0.08	0.16	0.01	0.01	0.59	0.14	260	258	3	275	266	12
		3	37.61	25.84	1.07	0.96	0.21	0.05	7.29	73.03	0.80	0.01	0.02	0.85	3.23	0.77	1.84	0.08	0.12	0.20	0.08	0.12	0.01	0.04	0.60	0.15	255			258		
1248	905.9	1	35.43	26.23	0.47	0.54	0.26	0.01	7.44	70.38	0.85	0.00	0.02	0.90	3.16	0.84	1.91	0.04	0.07	0.11	0.04	0.07	0.00	0.05	0.74	0.10	276			268		
		3	38.31	28.41	0.46	0.29	0.27	0.08	7.82	75.64	0.82	0.01	0.02	0.89	3.17	0.83	1.94	0.03	0.04	0.07	0.03	0.04	0.01	0.05	0.76	0.11	271	268	18	254	260	15
		4	38.89	28.25	0.51	0.50	0.27	0.04	7.24	75.70	0.76	0.01	0.02	0.81	3.20	0.80	1.93	0.04	0.06	0.10	0.04	0.06	0.01	0.05	0.66	0.19	242			242		
		6	35.49	26.41	0.54	0.71	0.20	0.02	7.62	70.99	0.86	0.00	0.02	0.90	3.14	0.86	1.90	0.04	0.09	0.13	0.04	0.09	0.00	0.04	0.73	0.10	278			276		
1249	915.0	6	37.34	26.71	0.50	0.36	0.12	0.02	6.99	72.04	0.77	0.00	0.01	0.80	3.22	0.78	1.94	0.04	0.05	0.08	0.04	0.05	0.00	0.02	0.69	0.20	235	235	0	240	240	0
1250	935.0	5	37.81	27.85	0.65	0.67	0.36	0.08	8.02	75.44	0.85	0.01	0.03	0.93	3.15	0.85	1.89	0.05	0.08	0.13	0.05	0.08	0.01	0.06	0.72	0.07	289	289	0	270	289	0
1252	975.6	2	40.66	29.32	0.61	0.40	0.17	0.03	8.21	79.40	0.82	0.00	0.01	0.86	3.20	0.80	1.92	0.04	0.05	0.09	0.04	0.05	0.00	0.03	0.74	0.14	260			254		
		3	39.31	29.21	0.57	0.57	0.21	0.02	8.23	78.12	0.84	0.00	0.02	0.88	3.15	0.85	1.92	0.04	0.07	0.11	0.04	0.07	0.00	0.04	0.74	0.12	270	265	5	265	257	8
		4	37.90	25.97	0.51	0.55	0.23	0.03	7.12	72.31	0.78	0.01	0.02	0.83	3.26	0.74	1.90	0.04	0.07	0.11	0.04	0.07	0.01	0.04	0.67	0.17	249			250		
1253	1001.7	1	35.41	26.04	0.47	0.42	0.14	0.04	7.67	70.19	0.88	0.01	0.01	0.91	3.17	0.83	1.91	0.04	0.06	0.09	0.04	0.06	0.01	0.03	0.78	0.09	281			272		
		4	35.76	26.78	0.41	0.33	0.12	0.02	7.41	70.83	0.83	0.00	0.01	0.86	3.16	0.84	1.94	0.03	0.04	0.07	0.03	0.04	0.00	0.02	0.76	0.14	261	274	13	259	264	7
		5	40.25	29.59	0.52	0.37	0.16	0.08	8.49	79.46	0.85	0.01	0.01	0.89	3.17	0.83	1.93	0.03	0.04	0.08	0.03	0.04	0.01	0.03	0.78	0.11	275			263		
1254	1021.3	1	42.70	31.17	0.62	0.49	0.28	0.07	9.00	84.33	0.85	0.01	0.02	0.91	3.18	0.82	1.91	0.04	0.05	0.09	0.04	0.05	0.01	0.04	0.76	0.09	281	278	3	265	267	3
		2	45.58	33.57	0.60	0.53	0.18	0.05	9.75	90.26	0.86	0.01	0.01	0.90	3.17	0.83	1.92	0.03	0.05	0.09	0.03	0.05	0.01	0.03	0.77	0.10	276			269		
1346	666.7	1	43.72	31.00	0.91	0.68	0.27	0.08	8.77	85.43	0.82	0.01	0.02	0.87	3.21	0.79	1.89	0.06	0.07	0.13	0.06	0.07	0.01	0.04	0.69	0.13	267			256		
		2	37.89	27.40	0.93	0.62	0.24	0.08	8.26	75.42	0.88	0.01	0.02	0.94	3.17	0.83	1.87	0.07	0.08	0.14	0.07	0.08	0.01	0.04	0.74	0.06	292			271		
		3	41.85	29.76	0.70	0.57	0.20	0.08	8.21	81.37	0.80	0.01	0.02	0.85	3.21	0.79	1.91	0.04	0.07	0.11	0.04	0.07	0.01	0.03	0.69	0.15	257	267	15	252	259	9
		4	41.09	29.27	0.83	0.57	0.16	0.08	8.21	80.21	0.82	0.01	0.01	0.86	3.21	0.79	1.90	0.05	0.07	0.12	0.05	0.07	0.01	0.03	0.70	0.14	260			254		
		5	44.22	30.76	0.79	0.66	0.20	0.06	8.49	85.18	0.79	0.01	0.02	0.83	3.24	0.76	1.90	0.05	0.07	0.12	0.05	0.07	0.01	0.03	0.67	0.17	250			250		
		6	41.11	29.28	1.12	0.91	0.22	0.04	8.69	81.37	0.86	0.01	0.02	0.90	3.18	0.82	1.85	0.07	0.11	0.18	0.07	0.11	0.01	0.04	0.68	0.10	277			270		
1349	765.3	3	44.34	29.73	1.05	1.02	0.25	0.06	7.65	84.10	0.72	0.01	0.02	0.77	3.28	0.72	1.87	0.06	0.11	0.18	0.06	0.11	0.01	0.04	0.54	0.23	225	239	20	237	246	13
		4	42.56	29.48	0.69	0.87	0.28	0.08	8.05	82.01	0.78	0.01	0.02	0.84	3.24	0.76	1.88	0.04	0.10	0.14	0.04	0.10	0.01	0.05	0.64	0.16	253			255		
1360	1007.5	1	36.45	27.38	0.72	0.58	0.11	0.06	7.91	73.21	0.87	0.01	0.01	0.90	3.13	0.87	1.91	0.05	0.07	0.13	0.05	0.07	0.01	0.02	0.74	0.10	276			270		
		4	38.04	27.06	0.69	0.33	0.27	0.18	7.42	73.99	0.80	0.03	0.02	0.88	3.21	0.79	1.91	0.05	0.04	0.09	0.05	0.04	0.03	0.05	0.71	0.12	268			248		
		5	47.43	34.61	0.81	0.51	0.13	0.09	10.00	93.58	0.86	0.01	0.01	0.89	3.18	0.82	1.91	0.05	0.05	0.10	0.05	0.05	0.01	0.02	0.76	0.11	271	272	12	262	260	9
		6	44.84	32.98	0.80	0.51	0.22	0.16	9.83	89.34	0.88	0.02	0.02	0.94	3.16	0.84	1.90	0.05	0.05	0.10	0.05	0.05	0.02	0.03	0.78	0.06	293			270		
		7	44.30	31.93	0.96	0.47	0.14	0.11	8.89	86.80	0.82	0.02	0.01	0.86	3.20	0.80	1.91	0.06	0.05	0.11	0.06	0.05	0.02	0.02	0.71	0.14	259			253		
		8	38.41	29.02	0.85	0.36	0.14	0.07	7.98	76.83	0.83	0.01	0.01	0.87	3.14	0.86	1.93	0.06	0.04	0.10	0.06	0.04	0.01	0.02	0.73	0.13	264			258		

IV – tetrahedral site; VI – octahedral site; IC – interlayer charge; R^{2+} – divalent cations. Fe-cel. = Fe-celadonite; Mg-cel. = Mg-celadonite; Par. = paragonite; Ca-par. = Ca-paragonite; Mus. = muscovite; Pyr. = pyrophyllite. [a] T1 was calculated using Cathelineau (1988)'s method while T2 was calculated using Battaglia (2004)'s method.

interpreted them as diagenetic temperatures. These temperatures overlap with the fluid inclusion homogenization temperatures and the illite temperatures obtained in this study. It is worth noting that all the illite examined in this study is hairy or needle-like, similar to the 1 Mt polytype described in previous studies, which is consistent with the relatively high temperatures estimated.

8.3. Thermal profiles and implications for fluid flow mechanisms

The fluid inclusion homogenization temperatures and calculated illite temperatures from the three drill cores examined in this study have wide ranges and do not show obvious trends of increase with depth (Fig. 10). The wide ranges of temperatures may be related to the complex diagenetic history of the Athabasca basin, as discussed above, whereas the temperature–depth distribution profiles may be related to geothermal gradients, maximum burial depths, and mechanisms of basinal fluid flow, which will be discussed below.

In old intracratonic basins, heat flow is generally stable and the maximum burial temperatures are almost linearly proportional to depths (e.g., Illinois basin: Graf et al., 1966; Michigan basin: Graf et al., 1966; Speece et al., 1985; Williston basin: Hanor, 1979; Gosnold et al., 2012), except some local thermal anomalies due to temporary thermal convection effects (Majorowicz and Jessop, 1986; Nunn, 1992). In the case of the Athabasca basin, a previous study of fluid inclusions in quartz overgrowths from the Rumpel Lake and MP-73-183 drill cores by Pagel (1975) estimated a geothermal gradient of 35 °C/km and a maximum burial depth of about 5 km. These estimates have since been used by many researchers (e.g. Hoeve and Quirt, 1984; Kotzer and Kyser, 1995; Cui et al., 2012a and b; Chi et al., 2013) to infer that as much as 5 km of strata have been eroded from above the preserved strata. However, it can be shown that there are some problems with Pagel's (1975) original estimation of geothermal gradients and burial depths, and that many recent paleo-geothermal data, including those documented in this study and by Kotzer and Kyser (1995); Stasiuk et al. (2001) and

Scott and Chi (2014), cannot be explained with Pagel's (1975) burial model.

Pagel's (1975) estimation of geothermal gradient and maximum burial depth is based on the assumption of a lthostatic fluid pressure system in the Athabasca basin and that the melting temperatures of halite in fluid inclusions represent the trapping temperatures. Numerical modeling of sediment compaction has shown that fluid pressures in intracratonic basins are likely to be close to hydrostatic values due to slow sedimentation over a prolonged geological time (Bethke, 1985), as is the case for the Athabasca basin (Chi et al., 2013). The sandstone dominated nature of the Athabsca basin further contributes to the development of a hydrostatic fluid pressure system rather than lithostatic (Chi et al., 2013). As to the melting temperatures of halite in fluid inclusions, it has been shown that halite crystals can be accidently trapped in fluid inclusions, rather than having formed a daughter mineral (Becker et al., 2008), in such situations the halite-melting temperatures cannot be used to represent trapping temperatures. In fact, if the halite is treated as daughter mineral, and if we accept the assumption of a hydrostatic fluid pressure regime, the calculation of fluid pressures with Pagel's (1975) data would lead to an estimation of 11 km of erosion and a geothermal gradient of 12 °C/km, both difficult to reconcile with the geological condition of the Athabasca basin.

An examination of the depth–temperature profiles coupled with different geothermal gradient–erosion thickness combinations (Fig. 10) reveals that the outlines of maximum fluid inclusion homogenization temperatures and minimum illite temperatures are close to the trends assuming 5 km erosion and 35 °C/km geothermal gradient or 3 km erosion and 55 °C/km geothermal gradient. This observation, together with uncertainties about erosion thickness and geothermal gradient as discussed above, indicates that either the fluid inclusion homogenization temperatures and the illite temperatures are not accurate enough to define geothermal gradients given the limited vertical extent being examined, or the geothermal gradients are small, as suggested by the broadly vertical distributions of the temperature data (Figs. 7, 9, 10a, and c). Furthermore, the high illite temperatures cannot be explained with a simple burial model unless an erosion of >5 km or a geothermal gradient much higher than 35 °C/km is assumed (Fig. 10).

Taking all these together, we postulate that the Athabasca basin experienced extensive thermal disturbance during its diagenetic history, which heated various parts of the basin to higher-than-normal temperatures and masked any regular geothermal patterns that might have existed. Thermal disturbances have been recognized in many types of mineralizing systems(especially MVT and SEDEX) in sedimentary basins, and has been related to various driving forces, including topographic relief, fluid overpressure, and thermal convections (Cathles and Smith, 1983; Anderson and Macqueen, 1988; Bethke and Marshak, 1990; Garven et al., 1993; Duddy et al., 1994; Deming, 1994; Garven and Raffensperger, 1997; Cathles and Adams, 2005; Ingebritsen and Appold, 2012; Chi, 2015). In the case of the Athabasca basin, overpressure-driven fluid flow may be excluded because the fluid pressures were likely to be near hydrostatic due to the sandstone-dominated nature and slow sedimentation (Chi et al., 2013), whereas the topography-driven fluid flow model lacks supports from unidirectional temperature change (suggested by the thermal profiles in this study) and stremline confugations (suggested by the numerical modeling results in Cui et al., 2010) related to fluid flow away from the mountains, as documented for the classical MVT deposits in North America (Bethke and Marshak, 1990; Garven et al., 1993; Garven and Raffensperger, 1997). Several numerical modeling studies (Raffensperger and Garven, 1995a; Cui et al., 2012a, b; Li et al., 2015) have indicated that free convection may have been developed in the Athabasca basin under normal geothermal gradients, in part due to the high permeabilities due to its sandstone-dominated nature. Furthermore, the presence of ca. 1644 Ma volcanic rocks in the Wolverine Point Formation within the Athabasca basin (Rainbird et al., 2007) and the ca. 1267 Ma post-Athabasca Mackenzie diabase dikes (LeCheminant and Heaman, 1989) indicate that forced convection may have also been locally developed in relation to heat anomalies.

The high illite temperatures and quasi-absence of thermal gradients in the vertical direction observed in this study may be best explained by fluid convection in the basin, as high fluid temperatures and steep isotherms are characteristic of the upwelling limbs of individual convection cells (Raffensperger and Garven, 1995a; Cui et al., 2012a, b; Li et al., 2015). On the other hand, lower-than-normal temperatures are expected to be developed in the downwelling limbs. The similarity of thermal profiles between different drill cores examined in this study (Fig. 10) may suggest that these localities are coincident with the sites of upwelling convection. Alternatively, it may be explained by shifting of convection cells through time, as illustrated in Fig. 11. A "low temperature" site associated with downwelling flow at one time may evolve into a "high temperature" site associated with upwelling flow at another time (Fig. 11). As a result, any part of the basin may have experienced both "high" and "low" temperatures in the diagenetic history, which may also explain the wide ranges of temperatures as discussed above. According to Cui et al. (2010), multiple layers of convection may be developed due to presence of low-permeability layers in the sedimentary sequence, which may also explain the overall homogeneous distribution of high fluid temperatures in the basin. In addition to the thermal effects, fluid convection may also explain the nearly uniform distributions of fluid salinities with depths (Fig. 8), as fluids of different initial salinities may be mixed during convection.

8.4. Implications for unconformity-related uranium mineralization

The fluid convection models discussed above have important implications for URU mineralization in the Athabasca basin, both in terms of fluid flow mechanisms and uranium sources. Although fluid convection has been proposed in previous studies as a plausible mechanism for fluid flow related to URU mineralization (Raffensperger and Garven, 1995a; Cui et al., 2012a, b; Li et al., 2015), these studies are based solely on numerical modeling. The results from this study provide the first independently obtained evidence that supports fluid convection in the Athabasca basin. Although not all the fluid convection cells are related to mineralization, the recognition of fluid convection in the central part of the Athabasca basin suggests that there is potential to find URU deposits in this part of the basin, as long as other conditions of mineralization (e.g., geochemical traps) are met.

Another issue regarding URU ore genesis is about the sources of uranium. There are two schools of thought: one believes that uranium was derived from the basin (Hoeve and Sibbald, 1978; Hoeve and Quirt, 1984; Kotzer and Kyser, 1995; Komninou and Sverjensky, 1996; Fayek and Kyser, 1997; Kyser et al., 2000), and the other advocates sources from the basement (Dahlkamp, 1978; Annesley and Madore, 1999; Hecht and Cuney, 2000; Cuney et al., 2003; Richard et al., 2010; Mercadier et al., 2013). Although it is beyond the scope of this paper to discuss the pros and cons of each school of thought, it is worth elaborating on the potential significance of basin-scale fluid convection for metal sources.

Two types of brines have been found in URU deposits, i.e., a Na-rich brine and a Ca-rich brine (Derome et al., 2005; Richard et al., 2010), and the Ca-rich brine has been interpreted to have resulted from reaction between an originally Na-rich basinal brine with the Ca-rich lithologies in the basement, which is further taken to support that uranium was sourced from the basement (Derome et al., 2005; Richard et al., 2010). This interpretation is based in part on the assumption that the lithologies in the Athbasca Basin were originally Ca-poor as they are today (mainly quartz arenite). However, the abundance of fluid inclusions in quartz overgrowths with ice-melting temperatures significantly lower than the eutectic point of the H_2O-NaCl system (−21.2 °C), as documented in this study (Table 1) and by Scott and Chi (2014), indicates that Ca-rich brines were well developed within the Athabasca basin, and not limited to the URU deposits. This may be taken to argue that

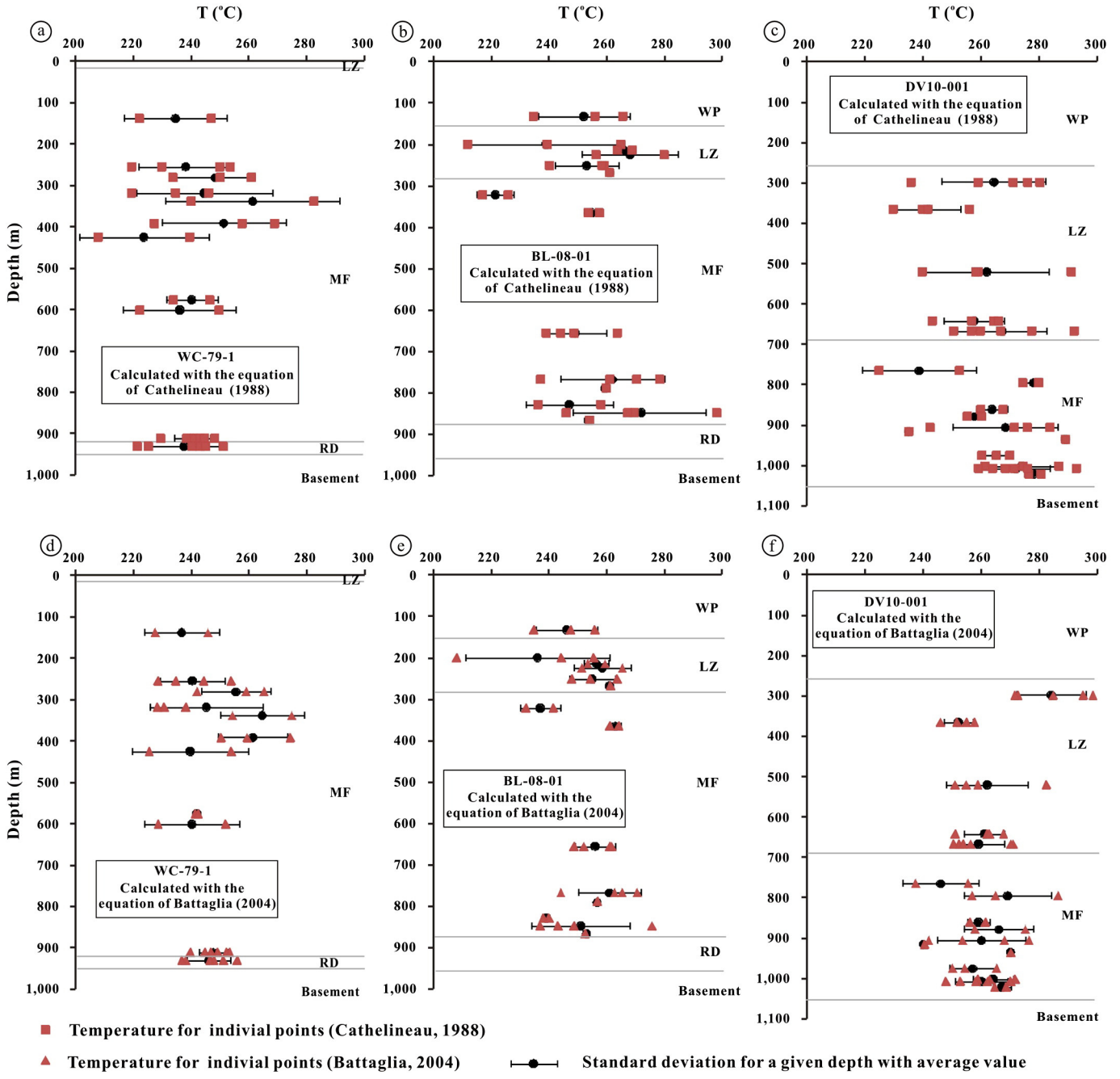

Fig. 9. Distribution of illite crystallization temperatures along depth from the drill cores WC-79-1, BL-08-01, and DV10-001. a, b, c — temperatures calculated using Cathelineau (1988)'s method; d, e, f — temperatures calculated using Battaglia (2004)'s method.

the lithologies of the Athabasca strata were originally more Ca-rich than today, and that Ca may have been released into the basinal fluids during diagenesis through fluid-rock interaction, as is proposed for the origin of most Ca-rich brines in sedimentary basins (Hanor, 1994). Alternatively, the development of Ca-rich brines in the basin may be used as evidence that fluid convection penetrated into the basement, as suggested by Cui et al. (2012b). Thus, Na-rich basinal brines infiltrated into the basement along the downwelling sites of convection cells, reacted with basement rocks and picked up Ca, and flowed back into the basin along the upwelling sites. The interpretation may explain the widespread bleaching of redbeds in the Athabasca basin, which is associated with dissolution of iron oxides and hydroxides due to introduction of relatively reducing fluids into the basin (Chu et al., 2015): these relatively reducing fluids may represent those returning from the basement driven by fluid convection.

Regardless of whether U and Ca were derived from the basement or the basin, the fluid convection processes will have facilitated fluid-rock interaction and metal extraction, as has been proposed in many sedimentary basins (Wood and Hewett, 1982, 1984; Bjorlykke et al., 1988; Bjorlykke, 1994; Bjorlykke and Gran, 1994; Metcalfe et al., 1994). Such fluid convection could have maintained for several millions of years by recycling the same amount of fluids (Cassan et al., 1981; Wood and Hewett, 1982, 1984; Davis et al., 1985). Although the timing and duration of fluid convection in the Athabasca basin are difficult to determine, and the exact role that fluid convection may have played in the formation of individual URU deposits is unknown, the development of

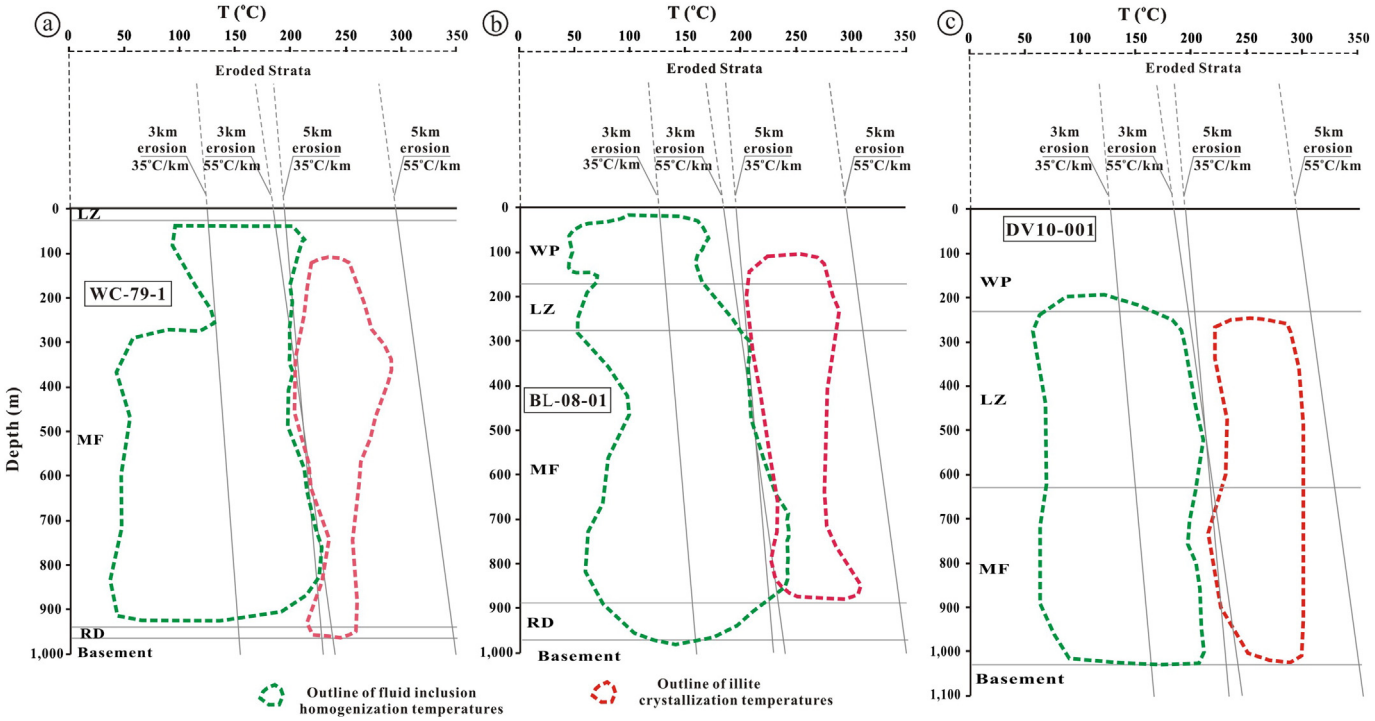

Fig. 10. Thermal profiles showing the outlines of fluid inclusion homogenization temperatures and illite crystallization temperatures (calculated using Cathelineau (1988)'s method) along depth of the WC-79-1, BL-08-01, and DV10-001 drill cores. Also shown are linear thermal profiles assuming thermal gradients of 35 °C/km and 55 °C/km, erosion thicknesses of 3 km and 5 km, and surface temperature of 20 °C.

basin-wide fluid convection processes, as suggested in this study, may be considered as a favorable indication of uranium mineralization for the basin as a whole, both in terms of the ground preparation (metal extraction and perhaps permeability enhancement) and fluid circulation required for mineralization.

9. Conclusions

Fluid inclusions in quartz overgrowths, and illite in interstitial space in sandstones from three drill cores (WC-79-1, BL-08-01, and DV10-001) located in the central part of the Athabasca basin, were studied to estimate the paleo-temperatures of basinal fluids in the diagenetic history of the basin. The fluid inclusions show homogenization temperatures from 50° to 235 °C, ice-melting temperatures from −9.2° to −48.6 °C (corresponding to salinities from 13.1 to 30.7 wt.%), and the illite crystallization temperatures range from 212° to 298 °C. The homogenization temperatures cover a wide range at any given depth, and do not show a systematic increase with depth. The illite temperatures are systematically higher than the fluid inclusion homogenization temperatures, and also do not show an obvious trend

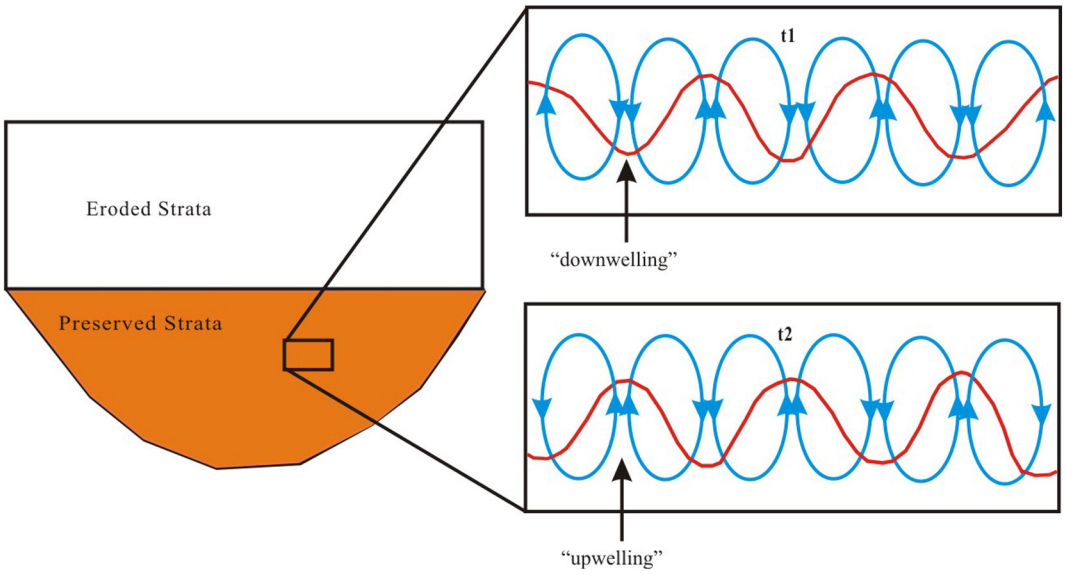

Fig. 11. A sketch showing how the whole basin may have been heated to higher-than-normal temperatures through shifting of fluid convection cells. A low temperature site associated with "downwelling" flow at one time (t1) may be overprinted by higher temperatures associated with "upwelling" flow at another time (t2).

of increase with depth. The ice-melting temperatures of fluid inclusions are mostly lower than −21.2 °C and there is no systematic change of fluid salinities with depth. There are no systematic differences in fluid inclusion homogenization temperatures, illite crystallization temperatures, and fluid compositions between the studied drill cores.

These results are interpreted to indicate that the Athabasca basin experienced thermal disturbances that raised the temperatures above those expected for a normal geothermal gradient (35 °C/km) during the long and complex diagenetic history. The quasi-absence of thermal gradients indicated by the thermal profiles documented in this study can be best explained by thermal convection. Although fluid convection has been proposed for the unconformity-related uranium deposits in the Athabasca basin in many previous studies, these studies are based solely on numerical modeling, and this study provide the first independently obtained evidence for fluid convection in the basin. The low ice-melting temperatures of fluid inclusions in the quartz overgrowths suggest that Ca-rich brines were developed in the basin, which may be interpreted to indicate either basin lithologies that were originally more Ca-rich than today, or that the fluid convection cells penetrated into the basement where Ca was extracted. Uranium required for unconformity-related uranium deposits may have been similarly derived either from the basin or the basement. In either case, fluid convection is considered favorable for uranium mineralization in terms of ground preparation (metal extraction and permeability enhancement) or fluid circulation.

Acknowledgment

This project is supported by an NSERC-Discovery Grant (to Chi). We would like to thank Sean Bosman and Colin Card from the Saskatchewan Geological Survey for assistance in sample collection and helpful discussion. Dr. Ravinder Sidhu from University of Manitoba is thanked for electron microprobe analysis. Constructive comments by two anonymous reviewers and Editor-in-Chief Dr. Franco Pirajno have greatly improved this paper, for which we are grateful.

References

Alexandre, P., Kyser, K., Thomas, D., Polito, P., Marlat, J., 2009. Geochronology of unconformity-related uranium deposits in the Athabasca Basin, Saskatchewan, Canada and their integration in the evolution of the basin. Mineral. Deposita 44, 41–59.

Alexandre, P., Kyser, T.K., 2012. Modeling of the fluid flow involved in the formation of Athabasca basin unconformity-type uranium deposits. Geological Association of Canada-Mineralogical Association of Canada Annual Conference Abstracts 35, p. 3.

Anderson, G.M., Macqueen, R.W., 1988. Mississippi valley-type lead-zinc deposits. In: Roberts, R.G., Sheahan, P.A. (Eds.), Ore Deposit Models. Geoscience Canada Reprint Series 3, pp. 79–90.

Annesley, I.R., Madore, C., 1999. Leucogranites and pegmatites of the sub-Athabasca basement, Saskatchewan: U protore? In: Stanley, C.J. (Ed.), Mineral Deposits: Processes to Processing. Balkema, Rotterdam, pp. 297–300

Annesley, I.R., Madore, C., Shi, R., Krogh, T.E., 1997. U-Pb geochronology of thermotectonic events in the Wollaston Lake area, Wollaston Domain: a summary of 1994–1996 results. Summary of Investigations. Saskatchewan Geological Survey, Saskatchewan Energy and Mines, Miscellaneous Report 97–4, pp. 162–173.

Bailey, E.H., Stevens, R.E., 1960. Selective Staining of Potash Feldspar and Plagioclase on Rock Slabs and Thin Sections. Am. Mineral. 45, 1020–1025.

Bakker, R.L., 2003. Package FLUIDS 1. Computer programs for analysis of fluid inclusion data and for modelling bulk fluid properties. Chem. Geol. 194, 3–23.

Battaglia, S., 2004. Variations in the chemical composition of illite from five geothermal fields: a possible geothermometer. Clay Miner. 39, 501–510.

Becker, S.P., Fall, A., Bodnar, R.J., 2008. Synthetic fluid inclusions. XVII. PVTX properties of high salinity H_2O–NaCl solutions (>30 wt.% NaCl): application to fluid inclusions that homogenize by halite disappearance from porphyry copper and other hydrothermal ore deposits. Econ. Geol. 103, 539–554.

Bethke, C.M., 1985. A numerical model of compaction-driven groundwater flow and heat transfer and its application to paleohydrology of intracratonic sedimentary basins. J. Geophys. Res. 90, 6817–6828.

Bethke, C.M., Marshak, S., 1990. Brine migration across North America — the plate tectonics of groundwater. Annu. Rev. Earth Planet. Sci. 18, 287–315.

Bjorlykke, K., 1994. Sedimentary fluid and diagenesis in sedimentary basins. In: Parnell, J. (Ed.), Geogluids: Origin, Migration and Evolution of Fluids in Sedimentary Basins. Geological Society, London, Special publication 78, pp. 127–140.

Bjorlykke, K., Gran, K., 1994. Salinity variations in North-Sea formation waters — implications for large-scale fluid movements. Mar. Pet. Geol. 11, 5–9.

Bjorlykke, K., Mo, A., Palm, E., 1988. Modelling of thermal convection in sedimentary basins and its relevance to diagenetic reactions. Mar. Pet. Geol. 5, 338–351.

Bodnar, R.J., Vityk, M.O., 1994. Interpretation of microthermometric data for H_2O–NaCl fluid inclusions. In: De Vivo, B., Frezzotti, M.L. (Eds.), Fluid Inclusions in Minerals: Methods and applications, Short Course of the working Group IMA "Inclusions in Minerals", pp. 117–130.

Boiron, M.-C., Cathelineau, M., Richard, A., 2010. Fluid flows and metal deposition near basement/cover Fluid flows and metal deposition near basement ⁄ cover unconformity: lessons and analogies from Pb–Zn–F–Ba systems for the understanding of Proterozoic U deposits. Geofluids 10, 270–292.

Bosman, S.A., Card, C.D., Brewster, Z., Fehr, C., 2011. The Athabasca Basin ore-systems project: a new generation of geosciences in the Athabasca Basin. Summary of Investigation, Saskatchewan Geological Survey, Miscellaneous Report 2011–4.2, Paper A–4 (9 pp.).

Bosman, S.A., Card, C.D., MacKnight, S.G., Boulanger, S., 2012. The Athabasca basin ore-systems project: an update on geochemistry, spatial data, and core logging. Summary of Investigation, Saskatchewan Geological Survey, Miscellaneous Report 2012–4.2, Paper A–5 (10 pp.).

Card, C.D., 2012. A proposed domainal reclassification for Saskatchewan's Hearne and Rae provinces. Summary of Investigations 2012, Saskatchewan Geological Survey, Sask. Ministry of the Economy, Misc. Rep. 2012–4.2, Paper A–11 (9 pp.).

Card, C.D., Pana, D., Portella, P., Thomas, D.J., Annesley, I.R., 2007. Basement rocks of the Athabasca basin, Saskatchewan and Alberta. In: Jefferson, C.W., Delaney, G. (Eds.), EXTECH IV: Geology and Uranium Exploration Technology of the Proterozoic Athabasca Basin, Saskatchewan and Alberta. Geological Survey of Canada Bulletin 588, pp. 69–87.

Cassan, J.P., Palacios, M.C.G., Fritz, B., Tardy, B., 1981. Diagenesis of sandstone reservoirs as shown by petrographical and geochemical analyses of oil bearing formations in the Gabon Basin. Bull. Cent. Rech. Elf Aquitaine 5, 113–135 (Pau Cedex, France).

Cathelineau, M., 1988. Cation site occupancy in chlorites and illites as a function of Temperature. Clay minerals 23, 471–485.

Cathles, L.M., Adams, J.J., 2005. Fluid flow and petroleum and mineral resources in the upper (<20 km) continental crust. In: Hedenquist, J.W., Thompson, J.F.H., Goldfarb, R.J., Richards, J.P. (Eds.), Economic Geology One Hundredth Anniversary Volume, Society of Economic Geologists, pp. 77–110.

Cathles, L.M., Smith, A.T., 1983. Thermal constraints on the formation of Mississippi Valley-type lead–zinc deposits and their implications for episodic basin dewatering and deposit genesis. Econ. Geol. 78, 983–1002.

Chi, G., 2015. Constraints from fluid inclusion studies on hydrodynamic models of mineralization. Acta Petrol. Sin. 31, 907–917.

Chi, G., Bosman, S., Card, C., 2011. Fluid flow models related to uranium mineralization in the Athabasca basin: a review and new insights. Saskatchewan Geological Survey Open House 2011, Saskatoon, Abstract Volume, p. 4.

Chi, G., Bosman, S., Card, C., 2013. Numerical modeling of fluid pressure regime in the Athabasca Basin and implications for fluid flow models related to the unconformity-type uranium mineralization. J. Geochem. Explor. 125, 8–19.

Chi, G., Giles, P.S., Williamson, M.A., Lavoie, D., Bertrand, R., 2003. Diagenetic history and porosity evolution of Upper Carboniferous sandstones from the Spring Valley #1 well, Maritimes Basin, Canada — implications for reservoir development. J. Geochem. Explor. 80, 171–191.

Chi, G., Li, Z., Bethune, K., 2014. Numerical modeling of hydrocarbon generation in the Douglas Formation of the Athabasca basin (Canada) and implications for unconformity-related uranium mineralization. J. Geochem. Explor. 144, 37–48.

Chi, G., Lu, H., 2008. Validation and representation of fluid inclusion microthermometric data using the fluid inclusion assemblage (FIA) concept. Acta Petrol. Sin. 24, 1945–1953 (In Chinese, with English Abstract).

Chi, G., Ni, P., 2007. Equations for calculation of NaCl/(NaCl + $CaCl_2$) ratios and salinities from hydrohalite-melting and ice-melting temperatures in the H_2O–NaCl–$CaCl_2$ system. Acta Petrol. Sin. 23, 33–37.

Chi, G., Xue, C., 2014. Hydrodynamic regime as major control on localization of uranium mineralization in sedimentary basins. Sci. China Earth Sci. 57, 2928–2933.

Chu, H., Chi, G., Bosman, S., Card, C., 2015. Diagenetic and geochemical studies of sandstones from drill core DV10-001 in the Athabasca basin, Canada, and implications for uranium mineralization. J. Geochem. Explor. 148, 206–230.

Creaser, R.A., Stasiuk, L.D., 2007. Depositional age of the Douglas Formation, northern Saskatchewan, determined by Re–Os geochronology. In: Jefferson, C.W., Delaney, G. (Eds.), EXTECH IV: Geology and Uranium Exploration Technology of the Proterozoic Athabasca Basin, Saskatchewan and Alberta. Geological Survey of Canada Bulletin 588, pp. 341–346.

Cui, T., Yang, J., Samson, I.M., 2010. Numerical modeling of hydrothermal fluid flow in the Paleoproterozoic Thelon Basin, Nunavut, Canada. J. Geochem. Explor. 106, 69–76.

Cui, T., Yang, J., Samson, I.M., 2012a. Tectonic deformation and fluid flow: implications for the formation of unconformity-related uranium deposits. Econ. Geol. 107, 147–163.

Cui, T., Yang, J., Samson, I.M., 2012b. Solute transport across basement/cover interfaces by buoyancy-driven thermohaline convection: implications for the formation of unconformity-related uranium deposits. Am. J. Sci. 312, 994–1027.

Cuney, M., Brouand, M., Cathelineau, M., Derome, D., Freiberger, R., Hecht, L., Kister, P., Lobaev, V., Lorilleux, G., Peiffert, C., Bastoul, A.M., 2003. What parameters control the high-grade-large tonnage of Proterozoic unconformity related uranium deposits? Proceedings of International Conference on Uranium Geochemistry, Nancy, France, pp. 123–126

Dahlkamp, F.J., 1978. Geological appraisal of the Key Lake U–Ni deposits, northern Saskatchewan. Econ. Geol. 73, 1430–1449.

Davis, S.H., Rosenblad, S., Wood, J.R., Hewett, T.A., 1985. Convective fluid flow and diagenetic patterns in domed sheets. Am. J. Sci. 285, 207–223.

Deming, D., 1994. Fluid flow and heat transport in the upper continental crust. In: Parnell, J. (Ed.), Geogluids: origin, migration and evolution of fluids in sedimentary basins. Geological Society, London, Special publication 78, pp. 27–43.
Derome, D., Cathelineau, M., Cuney, M., Fabre, C., Lhomme, T., 2005. Mixing of sodic and calcic brines and uranium deposition at McArthur River, Saskatchewan, Canada: A Raman and Laser-Induced Breakdown Spectroscopic study of fluid inclusions. Econ. Geol. 100, 1529–1545.
Drits, V.A., Weber, F., Salyn, A.L., Tsipursky, S.I., 1993. X-ray identification of one-layer illite varieties: application to the study of illites around uranium deposits of Canada. Clay Clay Miner. 41, 389–398.
Duddy, I.R., Green, P.F., Bray, R.J., Hegarty, K.A., 1994. Recognition of the thermal effects of fluid flow in sedimentary basins. In: Parnell, J. (Ed.), Geofluids: origin, migration and evolution of fluids in sedimentary basins. Geological Society, London, Special publication 78, pp. 325–346.
Essene, E.J., Peacor, D.R., 1995. Clay mineral thermometry — a critical perspective. Clay Clay Miner. 43, 540–553.
Fayek, M., 2013. Uranium ore deposits: a review. In: Burns, P.C., Sigmon, G. (Eds.), Uranium: Cradle to Grave. Mineralogical Association of Canada Short Course Series 43, pp. 121–147.
Fayek, M., Kyser, T.K., 1997. Characterization of multiple fluid-flow events and rare-earth-element mobility associated with formations of unconformity-type uranium deposits in the Athabasca Basin, Saskatchewan. Can. Mineral. 35, 627–658.
Fission Energy Corp., 2012. Davy Lake, SK: URL http://www.fission-energy.com/s/davylake.asp (accessed Oct 15, 2012).
Garven, G., Ge, S.M., Person, G.M., Sverjensky, D.A., 1993. Genesis of stratabound ore deposits in the mid-continent basins of North America. 1. The role of regional groundwater flow. Am. J. Sci. 293, 497–568.
Garven, G., Raffensperger, J.P., 1997. Hydrogeology and geochemistry of ore genesis in sedimentary basins. In: Barnes, H.L. (Ed.), Geochemistry of Hydrothermal Ore Deposits, third ed. John Wiley & Sons, New York, pp. 125–189.
Goldstein, R.H., Reynolds, T.J., 1994. Systematics of fluid inclusions in diagenetic minerals. SEPM Short Course 31, 1–199.
Gosnold, W.D., McDonald, M.R., Klenner, R., Merriam, D., 2012. Thermostratigraphy of the Williston Basin. GRC Trans. 36, 663–670.
Graf, D.L., Meents, W.F., Friedman, I., Shimp, N.F., 1966. The origin of saline formation waters, III: calcite chloride waters. Ill. State Geol. Surv. Circ. 397 (60 pp.).
Hanor, J.S., 1979. Sedimentary genesis of hydrothermal fluids. In: Barnes, H.L. (Ed.), Geochemistry of Hydrothermal Ore Deposits. John Wiley and Sons, New York, pp. 137–168.
Hanor, J.S., 1994. Origin of saline fluids in sedimentay basins. In: Parnell, J. (Ed.), Geofluids: Origin, Migration and Evolution of Fluids in Sedimentary Basins. Geological Society, London, Special publication 78, pp. 151–174.
Hecht, L., Cuney, M., 2000. Hydrothermal alteration of monazite in the Precambrian basement of the Athabasca Basin: implications for the genesis of unconformity-related deposits. Mineral. Deposita 35, 791–795.
Hiatt, E., Kyser, K., 2000. Links between depositional and diagenetic processes in basin analysis: porosity and permeability evolution in sedimentary rocks, Chapter 4. In: Kyser, K. (Ed.)Fluids and Basin Evolution: Short Course Series vol. 28. Mineralogical Association of Canada, pp. 63–92.
Hiatt, E., Kyser, K., 2007. Sequence stratigraphy, hydrostratigraphy, and mineralizing fluid flow in the Proterozoic Manitou Falls Formation, eastern Athabasca Basin,Saskatchewan. In: Jefferson, C.W., Delaney, G. (Eds.), EXTECH IV: Geology and Uranium Exploration Technology of the Proterozoic Athabasca Basin, Saskatchewan and Alberta. Geological Survey of Canada Bulletin 588, pp. 489–506.
Hiatt, E., Kyser, K., Fayek, M., Polito, P., Holk, G.J., Riciputi, L.R., 2007. Early quartz cements and evolution of paleohydraulic properties of basal sandstones in three Paleoproterozoic continental basins: evidence from in situ $\delta^{18}O$ analysis of quartz cements. Chem. Geol. 238, 19–37.
Hiemstra, E.J., Goldstein, R.H., 2005. The diagenesis and fluid migration history of the Indian Basin Field, Eddy County, New Mexico. In: Lufholm, P., Cox, D. (Eds.), WTGS Publication 05–115 "Unconventional Reservoirs, Technologies, and Strategies, New Perspectives for the Permian Basin", pp. 197–206.
Hoeve, J., Quirt, D.H., 1984. Mineralization and host rock alteration in relation to clay mineral diagenesis and evolution of the middle-Proterozoic, Athabasca Basin, northern Saskatchewan, Canada. Saskatchewan Research Council, SRC Technical Report 187. Saskatchewan Research Council, p. 187.
Hoeve, J., Quirt, D.H., 1987. A stationary redox front as a critical factor in the formation of high-grade, unconformity-type uranium ores in the Athabasca Basin, Saskatchewan, Canada. Bull. Mineral. 110, 157–171.
Hoeve, J., Sibbald, T., 1978. On the genesis of Rabbit Lake and other unconformity-type uranium deposits in northern Saskatchewan, Canada. Econ. Geol. 73, 1450–1473.
Hoffman, P.F., 1988. United plates of America, the birth of a craton: early Proterozoic assembly and growth of Laurentia. Annu. Rev. Earth Planet. Sci. 16, 543–603.
Ingebritsen, S.E., Appold, M.S., 2012. The physical hydrogeology of ore deposits. Econ. Geol. 107, 559–584.
Jefferson, C.W., Thomas, D.J., Gandhi, S.S., Ramaekers, P., Delaney, G., Brisbin, D., Cutts, C., Portella, P., Olson, R.A., 2007. Unconformity-associated uranium deposits of the Athabasca Basin, Saskatchewan and Alberta. In: Jefferson, C.W., Delaney, G. (Eds.), EXTECH IV: geology and uranium exploration technology of the Proterozoic Athabasca Basin, Saskatchewan and Alberta. Geological Survey of Canada, Bulletin 588, pp. 23–68.
Jessop, A.M., Majorowicz, J.A., 1994. Fluid flow and heat transfer in sedimentary basins. *In*: Parnell, J. (Ed.,), Geogluids: origin, migration and evolution of fluids in sedimentary basins. Geol. Soc. Lond. Spec. Publ. 78, 43–54.
Kister, P., Laverret, E., Quirt, D., Cuney, M., Patrier, P., Beaufort, D., Bruneton, P., 2006. Mineralogy and geochemistry of the host–rock alterations associated to the Shea Creek unconformity-type uranium deposits (Saskatchewan, Canada), Part 2. Spatial distribution of the Athabasca Group sandstone matrix minerals. Clay Clay Miner. 54, 295–313.
Kister, P., Viellard, P., Cuney, M., Quirt, D.H., Laverret, E., 2005. Thermodynamic constraints on the mineralogical and fluid composition evolution in a clastic sedimentary basin: the Athabasca Basin (Saskatchewan, Canada). Eur. J. Mineral. 17, 325–342.
Knight, C.L., Bodnar, R.J., 1989. Synthetic fluid inclusions. IX: critical PVTX properties of $NaCl–H_2O$ solutions. Geochim. Cosmochim. Acta 53, 3–8.
Komninou, A., Sverjensky, D., 1996. Geochemical modeling of the formation of an unconformity-type uranium deposit. Econ. Geol. 91, 590–606.
Kotzer, T., Kyser, T., 1995. Petrogenesis of the Proterozoic Athabasca Basin, northern Saskatchewan, Canada, and its relation to diagenesis, hydrothermal uranium mineralization and paleohydrogeology. Chem. Geol. 120, 45–89.
Kotzer, T., Kyser, T., 1990. Fluid history of the Athabasca Basin and its relation to uranium deposits. Summary of Investigations 1990. Saskatchewan Geological Survey, Saskatchewan Energy and Mines, Miscellaneous Report 90–4 (pp. 153–l 57).
Kyser, K., Hiatt, E., Renac, C., Durocher, K., Holk, G., Deckart, K., 2000. Diagenetic fluids in Paleo- and Mesoproterozoic sedimentary basins and their implications for long protracted fluid histories, Chapter 10. In: Kyser, K. (Ed.)Fluids and basin evolution, Short Course Series vol. 28. Mineralogical Association of Canada, pp. 225–262.
Kyser, T.K., Cuney, M., 2008. Unconformity-related uranium deposits. In: Cuney, M., Kyser, M. (Eds.), Recent and Not-So-Recent Developments in Uranium Deposits and Implications for Exploration. Mineralogical Association of Canada Short Course Series 39, pp. 161–220.
Laverret, E., Patrier Mas, P., Beaufort, D., Kister, P., Quirt, D., Bruneton, P., Clauer, N., 2006. Mineralogy and geochemistry of the host-rock alterations associated with the Shea Creek unconformity-type uranium deposits (Athabasca Basin, Saskatchewan, Canada) Part 1. Spatial variation of illite properties. Clay Clay Miner. 54, 275–294.
LeCheminant, A., Heaman, L., 1989. Mackenzie igneous events, Canada: middle Proterozoic hotspot magmatism associated with ocean opening. Earth Planet. Sci. Lett. 96, 38–48.
Li, Z., Chi, G., Bethune, K., Bosman, S., Card, C., 2015. Geometric and hydrodynamic modelling and fluid–structural relationships in the southeastern Athabasca Basin and significance for uranium mineralization. Geol. Surv. Can. Open File 7791, 103–114.
Majorowicz, J.A., Jessop, A.M., 1986. Geothemics of the Williston Basin in Canada in relation to hydrodynamics and hydrocarbon occurrences. Geophysics 51, 767–779.
Mercadier, J., Annesley, I.R., McKechnie, C.L., Bogdan, T.S., Creighton, S., 2013. Magmatic and metamorphic uraninite mineralization in the western margin of the Trans-Hudson Orogen (Saskatchewan, Canada): major protores for unconformity-related uranium deposits. Econ. Geol. 108, 1037–1065.
Mercadier, J., Richard, A., Cathelinea, M., 2012. Boron- and magnesium-rich marine brines at the origin of giant unconformity-related uranium deposits: $\delta^{11}B$ evidence from Mg-tourmalines. Geology 40, 231–234.
Metcalfe, R., Rochelle, C.A., Savage, D., Higgo, J.W., 1994. Fluid-rock interactions during continental red bed diagenesis: implications for theoretical models of mineralization in sedimentary basins. Geol. Soc. Lond., Spec. Publ. 78, 301–324.
Nunn, J.A., 1992. Free thermal convection beneath the Michigan basin: thermal and subsidence effects (Abstract). EOS 73/43 Suppl. 547.
Oakes, C.S., Bodnar, R.J., Simonson, J.M., 1990. The system $NaCl–CaCl_2–H_2O$: I. The ice liquidus at 1 atm total pressure. Geochim. Cosmochim. Acta 54, 603–610.
Orrell, S.E., Bickford, M.E., Lewry, J.F., 1999. Crustal evolution and age of thermotectonic reworking in the western hinterland of Trans–Hudson Orogen, northern Saskatchewan. Precambrian Res. 95, 187–223.
Pagel, M., 1975. Détermination des conditions physico–chimiques de la silici fication diagénétique des grès Athabasca (Canada) au moyen des inclusions fluids. C. R. Acad. Sci. Paris 280, 2301–2304.
Pagel, M., Poty, B., Sheppard, S.M.F., 1980. Contribution to some Saskatchewan uranium deposits mainly from fluid inclusion and isotopic data. In: Ferguson, J., Goleby, A. (Eds.), Uranium in the Pine Creek Geosyncline. International Atomic Energy Agency (IAEA), Vienna, pp. 639–645.
Phillips, O.M., 2009. Geological Fluid Dynamics: Subsurface Flow and Reactions. Cambridge University Press, Cambridge, UK (285 pp.).
Quirt, D.H., 2010. Is illite still a pathfinder mineral for the geological environment of Athabasca unconformity-type uranium deposits? GeoCanada 2010 Conference, Calgary, May 10–14
Raffensperger, J.P., Garven, G., 1995a. The formation of unconformity-type uranium ore deposits 2. Coupled hydrochemical modeling. Am. J. Sci. 295, 639–696.
Raffensperger, J.P., Garven, G., 1995b. The formation of unconformity-type uranium ore deposits 1. Coupled groundwater flow and heat transport modeling. Am. J. Sci. 295, 581–636.
Rainbird, R.H., Stern, R.A., Rayner, N., Jefferson, C.W., 2006. Ar–Ar and U–Pb geochronology of a Late Paleoproterozoic rift basin: support for a genetic link with Hudsonian orogenesis, western Churchill Province, Nunavut, Canada. J. Geol. 114, 1–17.
Rainbird, R.H., Stern, R.A., Rayner, N., Jefferson, C.W., 2007. Age, provenance, and regional correlation of the Athabasca Group, Saskatchewan and Alberta, constrained by igneous and detrital zircon geochronology. In: Jefferson, C.W., Delaney, G. (Eds.), EXTECH IV: Geology and Uranium Exploration Technology of the Proterozoic Athabasca Basin, Saskatchewan and Alberta. Geological Survey of Canada Bulletin 588, pp. 193–209.
Ramaekers, P., Jefferson, C.W., Yeo, G.M., Collier, B., Long, D.G., Catuneanu, O., Bernier, S., Kupsch, B., Post, R., Drever, G., McHardy, S., Jircka, D., Cutts, C., Wheatley, K., 2007. Revised geological map and stratigraphy of the Athabasca Group, Saskatchewan and Alberta. In: Jefferson, C.W., Delaney, G. (Eds.), EXTECH IV: Geology and Exploration Technology of the Proterozoic Athabasca basin, Saskatchewan and Alberta. Geological Survey of Canada Bulletin 588, pp. 155–191.
Richard, A., Banks, D., Mercadier, J., Boiron, M., Cuney, M., Cathelineau, M., 2011. An evaporated seawater origin for the ore-forming brines in unconformity-related uranium

deposits (Athabasca Basin, Canada): Cl/Br and delta $\delta^{37}Cl$ analysis of fluid inclusions. Geochim. Cosmochim. Acta 75, 2792–2810.
Richard, A., Kendrick, M.A., Cathelineau, M., 2014. Noble gases (Ar, Kr, Xe) and halogens (Cl, Br, I) in fluid inclusions from the Athabasca Basin (Canada): implications for unconformity-related U deposits. Precambrian Res. 247, 110–125.
Richard, A., Pettke, T., Cathelineau, M., Boiron, M.-C., Mercadier, M., Cuney, M., Derome, D., 2010. Brine-rock interaction in the Athabasca basement (McArthur River U deposit, Canada): consequences for fluid chemistry and uranium uptake. Terra Nova 22, 303–308.
Roedder, E., 1984. Fluid inclusions. Mineralogical Society of America. Rev. Mineral. 12 (644 pp.).
Sanford, R.F., 1992. A new model for tabular-type uranium deposits. Econ. Geol. 87, 2041–2055.
Scott, R., Chi, G., 2014. Abnormal geothermal gradients and development of calcic brine in the Athabasca Basin and their importance for unconformity-type uranium mineralization. Goldschmidt 2014 Abstract, p. 2239.
Speece, M.A., Bowen, T.D., Folcik, J.L., Pollack, H.N., 1985. Analysis of temperatures in sedimentary basins: the Michigan Basin. Geophysics 50, 1318–1334.
Stasiuk, L.D., Fowler, M.G., Jiricka, D., Mossisson, D., Sopuck, V., Wheatley, K., Wilson, N.S., Zaluski, G., 2001. Preliminary investigation into organic petrology and organic geochemistry of Proterozoic Douglas Formation shales and Athabasca Group sandstones distal and proximal to uranium mineralization, Athabasca basin, Saskatchewan. Summary of Investigations 2001, Volume 2, Saskatchewan Geological Survey, Saskatchewan Energy and Mines, Miscellaneous Report 2001–4.2, pp. 224–239.
Steele-MacInnis, M., Bodnar, R.J., Naden, J., 2011. Numerical model to determine the composition of H_2O–NaCl–$CaCl_2$ fluid inclusions based on microthermometric and microanalytical data. Geochim. Cosmochim. Acta 75, 21–40.
Wilson, M.R., Kyser, K., 1987. Stable isotopes geochemistry of alteration associated with the Key Lake uranium deposit, Canada. Econ. Geol. 82, 1540–1557.
Wood, J.R., Hewett, T.A., 1984. Reservoir diagenesis and convective fluid flow. In: McDonald, D.A., Surdam, R.C. (Eds.), Clastic Diagenesis. American Association Petroleum Geologists Memoir 37, pp. 99–110.
Wood, J.R., Hewett, T.A., 1982. Fluid convection and mass transfer in porous sandstones—a theoretical model. Geochim. Cosmochim. Acta 46, 1707–1713.
Zhang, Y.G., Frantz, J.D., 1987. Determination of the homogenization temperatures and densities of supercritical fluids in the system NaCl–KCl–$CaCl_2$–H_2O using synthetic fluid inclusions. Chem. Geol. 64, 335–350.